Preprint
UCRL-JC-134924

Modeling of the Competition of Stimulated Raman and Brillouin Scatter in LULI Multiple Beam Experiments

B.I. Cohen, H.A. Baldis, R.L. Berger, K.G. Estabrook, E.A. Williams and C. Labaune

This article was submitted to Physics of Plasmas

June 13, 2000

U.S. Department of Energy
Lawrence Livermore National Laboratory

Approved for public release; further dissemination unlimited

Modeling of the Competition of Stimulated Raman and Brillouin Scatter in Multiple Beam Experiments

Bruce I. Cohen and Hector A. Baldis

Institute for Laser Science and Applications

University of California Lawrence Livermore National Laboratory,

Livermore, California 94550

Richard L. Berger, Kent G. Estabrook, and Edward A. Williams

University of California Lawrence Livermore National Laboratory,

Livermore, California 94550

Christine Labaune

Laboratoire pour L'Utilisation des Lasers Intenses, CNRS, Ecole Polytechnique

91228 Palaiseau, France

*This work was performed for the U.S. Department of Energy under Contract No. W-7405-ENG-48 at the University of California Lawrence Livermore National Laboratory partly through the Institute for Laser Science and Applications.

Abstract

Multiple laser beam experiments with plastic target foils at the Laboratoire pour L'Utilisation des Lasers Intenses (LULI) facility [Baldis, *et al*., Phys. Rev. Lett. **77**, 2957 (1996)] demonstrated anti-correlation of stimulated Brillouin and Raman backscatter (SBS and SRS). Detailed Thomson scattering diagnostics showed that SBS always precedes SRS, that secondary electron plasma waves sometimes accompanied SRS appropriate to the Langmuir Decay Instability (LDI), and that, with multiple interaction laser beams, the SBS direct backscatter signal in the primary laser beam was reduced while the SRS backscatter signal was enhanced and occurred earlier in time. Analysis and numerical calculations are presented here that evaluate the influences on the competition of SBS and SRS, of local pump depletion in laser hot spots due to SBS, of mode coupling of SBS and LDI ion waves, and of optical mixing of secondary and primary laser beams . These influences can be significant. The calculations take into account simple models of the laser beam hot-spot intensity probability distributions and assess whether ponderomotive and thermal self-focusing are significant. Within the limits of the model, which omits several other potentially important nonlinearities, the calculations suggest the effectiveness of local pump depletion, ion wave mode coupling, and optical mixing in affecting the LULI observations.

PACS numbers: 52.40.Nk,52.58.Ns,52.35Mw

I. INTRODUCTION

Laser-plasma experiments at the Laboratoire pour L'Utilisation des Lasers Intenses (LULI)[1-7] have yielded a number of interesting observations bearing on the physics of stimulated Brillouin (SBS) and Raman (SRS) scattering. Of particular interest have been observations of the anti-correlation of SBS and SRS in multiple-beam experiments with exploding CH (carbon and hydrogen plastic) foils.[6-7] The anti-correlation of SBS and SRS has also been observed in other experiments[8] and in simulations.[9] In all of the LULI experiments where there is evidence of both SBS and SRS during a single shot, the peak of the SBS signals preceded the SRS signals in time; and the SBS signals emanated from closer to the expanding edge of the plasma. Moreover, with the addition of a second and a third interaction laser beam, the tendency was for the SBS direct backscatter to saturate sooner in time and at a lower amplitude (both in the ion acoustic wave's electron density perturbation and the reflectivity), and for the SRS backscatter to onset sooner and at a higher amplitude (Figs. 1-5). With two interaction beams at 22.5˚ relative angle, the observed SBS ion acoustic wave's electron density perturbation associated with the ion wave bisecting the laser propagation directions (the mutually resonant ion wave) increased in amplitude with increasing intensity of the two driving waves.[6] Observations in the LULI experiments also indicated that the peak of the SRS signals did not generally occur at the peak of electron density profile[2] and that electron plasma waves associated with Langmuir Decay Instability (LDI) were observed accompanying strong SRS activity.[5] These experimental results and their explanation are of continuing interest.

More generally, the study of and control of SBS and SRS have received continuous theoretical and experimental attention for many years in laser fusion research.[1-14] The symmetric compression of fusion targets in either direct drive or indirect drive can be affected by SBS and SRS, and there is the potential for damage to plasma-facing optics from direct backscatter unless these instabilities are controlled.[15] Furthermore, the optimization of the fusion performance of experiments in multiple beam facilities like the National Ignition Facility (NIF)[16] requires careful control over both the timing and relative amplitudes of the crossing beams, which sets limits on how

much SBS and SRS can be tolerated. Finally, understanding the nonlinear aspects of SBS and SRS is of continuing fundamental interest.

In a previous paper[17] we used BZOHAR two-dimensional, hybrid (particle ions and Boltzmann fluid electrons) simulations and an analytical model describing SBS and ion wave mode coupling to model aspects of the nonlinear interaction of SBS in a plasma with two laser interaction beams. In this previous work it was demonstrated how the SBS driven ion wave from a secondary laser interaction beam can mode-couple with the ion wave due to SBS backscatter of the primary laser beam leading to enhanced dissipation for the primary ion wave and partial suppression of the direct SBS backscatter of the primary interaction beam. However, the simple model used in Ref. 17 did not include the nonuniformity of laser beams due to random phase plates, the back-reaction of the ion wave mode coupling on both the primary and secondary SBS ion waves, and mode coupling with the mutually resonant ion wave driven by both interaction beams. Moreover, the possible mode coupling of the SBS-driven ion waves and the ion waves associated with LDI was also omitted in Ref. 17. This work addresses some of the physics associated with the competition of SBS and SRS in experiments with multiple laser beams. There have been many studies of the competition and anti-correlation between SBS and SRS for a single laser beam.[18-22]

The present study extends the modeling in Ref. 17 in a number of important ways. We have undertaken a more complete and self-consistent treatment of the ion wave mode coupling including coupling to the LDI ion wave and including probability distribution functions for the laser beam speckle intensity statistics. If the SBS and SRS overlap in space-time, the mode coupling analysis presented here indicates that ion wave mode coupling contributes to giving a stronger SRS signal because it leads to enhanced dissipation in both the LDI ion and the SBS ion waves, and because LDI is an important SRS saturation mechanism in the intense speckles. Including the laser beam nonuniformities is important because the parametric instabilities and secondary nonlinear processes occur preferentially in regions of high intensity. In addition to evaluating ion wave mode coupling in more detail in the present study, there is a calculation of pump depletion of the primary interaction beam due to the mutually resonant SBS process when a second interaction beam is

present. For LULI parameters most of the SBS and SRS occurs in intense speckles,[23] and averaging over the speckle intensity distribution functions indicates that there is little SBS pump depletion averaged over the beam (a few percent or less). However, we demonstrate here that local pump depletion in intense speckles due to mutually resonant SBS is significant for LULI parameters (and due to SBS direct backscatter when only one interaction beam is present) and increases with the intensity of the secondary interaction beam. This reduces the laser pump intensity available for SBS direct backscatter and for SRS farther into the plasma in the same speckle. This is qualitatively consistent with LULI observations of the partial suppression of SBS backscatter in the primary beam and with the relative weakness of the SRS signals when SBS is strong. When the SBS is partially suppressed and its saturation is accomplished earlier in time in a shot, there is more laser intensity available for exciting SRS farther into the plasma following the quenching of SBS in the intense speckles; and the SRS will onset sooner and likely achieve higher amplitudes. Our calculations suggest that local pump depletion in intense speckles may be a stronger effect than ion wave mode coupling in the LULI observations. (In our earlier modeling of the anti-correlation of SBS and SRS in LULI multiple-beam experiments, we gave no consideration to local pump depletion in intense speckles and only examined some of the physics of nonlinear ion wave mode coupling.[7,17])

Finally, we consider the possibilty that with two interaction beams there may be a three-wave SBS resonance (SBS optical mixing[24-28]) in a local drift frame in the expanding plasma. Such a resonance could allow wave energy transfer from the primary beam to the secondary beam which would also limit the direct SBS backscatter of the primary beam. However, if there is a resonance, the energy transfer can be limited by spatial gradients of the plasma flow and detuned by fluctuations in the plasma drift velocity, the electron temperature, or the electron density. A quantitative calculation of the potential for optical mixing (in which laser energy can be transferred from one interaction beam to a second beam) is presented.

The analysis and modeling of the LULI multiple beam experiments given here is selective in nature, and the model is simplified in several respects. To make progress in understanding some of

the nonlinear aspects of the complex observations in these experiments, we have focussed on a limited set of nonlinear mechanisms that can influence the competition and anti-correlation of SBS and SRS, i.e., local pump depletion in intense speckles, ion wave mode coupling, and SBS optical mixing. Within the framework of the relatively simple models used, the analysis is quantitative. However, we do not have a complete experimental knowledge of all of the plasma properties that influence the nonlinear interactions; and the models do not attempt to include all nonlinearities. Furthermore, some of the model simplifications give results for specific phenomena that differ with the results of more complete models, which we will identify. In addition, the incorporation of additional nonlinearities would not be additive; and the relative quantitative importance of the nonlinearities included in this study could be altered by the inclusion of additional nonlinear physics in a more comprehensive model. Nevertheless, there is a sufficient degree of semi-quantitative agreement between our model calculations and the LULI observations to suggest that both local pump depletion in intense speckles and ion wave mode coupling can contribute significantly.

The paper is organized as follows. In Section II we provide the analytical formulation of our mode coupling analysis of SBS, SRS, and LDI. We present an analytical reduction of the SBS, SRS, and LDI coupled equations in Sec. III and describe the linear SBS and SRS conditions for LULI parameters. In this analysis we include evaluations of the possible absolute instability of SRS at the density maximum of the plasma and of thermal and ponderomotive self-focusing in the LULI plasmas. Theory suggests that there is self-focusing of intense speckles in LULI. Analyses of local pump depletion in intense speckles for single-beam SBS and two-beam mutually resonant SBS are presented in Sec. IV. We average the local pump depletion over model speckle intensity distributions to determine beam-averaged pump depletions. The influences of two-beam mutually resonant SBS pump depletion on SBS direct backscatter and on SRS in the primary interaction beam are calculated. In Sec. V we calculate the partial suppression of SBS direct backscatter in the primary interaction beam due to ion wave mode coupling in the presence of the secondary laser beam taking into account model speckle intensity distributions. We also calculate the enhanced

dissipation experienced by LDI in the presence of SBS due to ion wave mode coupling and the concomitant enhancement of SRS taking into account model speckle intensity distributions. An analysis of the potential for energy transfer by two crossing interaction beams due to near-forward SBS scattering in the LULI experiments is given in Sec. VI. Concluding remarks are presented in Sec. VII.

II. ANALYTICAL FORMULATION: PARAMETRIC INSTABILITIES AND MODE COUPLING

Here we introduce a formulation of the nonlinear coupled mode equations that includes SBS, SRS, LDI, and ion wave mode coupling. These coupled mode equations are derived straightforwardly from the coupled nonlinear plasma dynamical equations (Vlasov or fluid) and Maxwell's equations for the self-consistent electromagnetic fields.[10-13] As is standard practice in parametric instability analyses, we introduce slowly varying wave amplitudes (temporal and spatial variations that are slow compared to the characteristic frequencies and wavelengths of the normal modes) and then, to simplify further, consider only variations of the wave envelopes in one spatial dimension (variation in the direction of propagation of the primary laser interaction beam normal to the exploding foil, which is the same direction as the principal inhomogeneities in the expanding plasma). Geometrical factors associated with the angle between the primary and secondary laser interaction beams are retained, which affect certain convective derivatives and coupling coefficients. The strong variation of laser speckle intensities perpendicular to the primary propagation direction is mocked up by introducing a probability distribution for the speckle intensity distribution in Sec. IVB. We also assume that many of the beat waves in the plasma are heavily damped and look for steady-state solutions ($\partial/\partial t=0$) of the equations and neglect convective (total) time derivatives where indicated.

Stimulated Raman backscatter is described by

$$-\mathrm{v}_{gR}\frac{\partial a_{1R}}{\partial x} = id_1 a_0^* a_{L1} - \gamma_{1R} a_{1R} \tag{1a}$$

$$\mathrm{v}_{gL1}\frac{\partial a_{L1}}{\partial x} = -id_2 a_0 a_{1R} - (\gamma_{L1} + i\Delta_{L1}(x))a_{L1} + id_3 a_{sLD} a_{L2} \approx 0 \tag{1b}$$

where a_0 represents the primary laser pump amplitude (complex valued in general), a_{1R} is the backscatter transverse wave amplitude, v_{gR} is the group velocity of the backscatter light. Langmuir decay instability excited by the SRS-produced Langmuir wave a_{L1} is given by

$$-v_{gL2}\frac{\partial a_{L2}}{\partial x} = -id_4 a_{L1}^{*} a_{sLD} - \gamma_{L2} a_{L2} \tag{2a}$$

$$\frac{da_{sLD}}{dt} = id_5 a_{L1} a_{L2} - (\gamma_{sLD} + i\Delta_{sLD}(x)) a_{sLD} - \sum_s ic_{LD} a_s a_{sLD+s} = 0 \tag{2b}$$

$$\frac{da_{sLD+s}}{dt} = -ic_{LD+s} a_s a_{sLD} - (\gamma_{sLD+s} + i\Delta_{sLD+s}(x)) a_{sLD+s} = 0 \tag{2c}$$

where a_{L2} is the backward propagating Langmuir decay wave, a_{sLD} is the ion wave amplitude associated with LDI, and a_s and a_{sLD+s} represent the amplitudes of other ion waves that beat with one another to couple to a_{sLD} (in our computation we sum over these wave couplings).

Stimulated Brillouin backscatter by the first (primary) interaction beam is represented by

$$-v_{gB}\frac{\partial a_{1B}}{\partial x} = ic_1 a_0 a_{s1} - \gamma_{1B} a_{1B} \tag{3a}$$

$$\frac{da_{s1}}{dt} = -ic_2 a_0 a_{1B} - (\gamma_{s1} + i\Delta_{s1}(x)) a_{s1} - \sum_s ic_{b1} a_s a_{s1+s} = 0 \tag{3b}$$

$$\frac{da_{s1+s}}{dt} = -ic_{s1+s} a_{s1} a_s - (\gamma_{s1+s} + i\Delta_{s1+s}(x)) a_{s1+s} = 0 \tag{3c}$$

where a_s represents other ion waves and a_{s1-s} represents the ion acoustic beat waves generated by a_{s1} beating with a_s. There is a second SBS backscatter process associated with a second interaction beam introduced at a small relative angle to the first interaction beam, and this SBS interaction produces an ion acoustic wave with amplitude a_{s2}. The equations describing the SBS backscatter of the second beam are entirely analogous to Eqs.(3a-3c). With two interaction beams present there is an SBS interaction driving an ion wave propagating in the direction bisecting the two angles of propagation of the two laser beams.[6] This SBS interaction produces a "mutually resonant" ion wave with amplitude a_{sr} described by the following equations:

$$-v_{gB}\cos\theta\frac{\partial a_{1Br}}{\partial x} = ic_1 a_0^{*} a_{sr} - \gamma_{1Br} a_{1Br} \tag{4a}$$

$$-v_{gB}\frac{\partial a_{2Br}}{\partial x} = ic_1 a_{0sd}^{*} a_{sr} - \gamma_{2Br} a_{2Br} \tag{4b}$$

$$\frac{da_{sr}}{dt} = -ic_{2r}(a_0 a_{1Br} + a_{0sd} a_{2Br}) - (\gamma_{sr} + i\Delta_{sr}(x)) a_{sr} - \sum_s ic_r a_s a_{sr+s} = 0 \tag{4c}$$

$$\frac{da_{sr+s}}{dt} = -ic_{sr+s}a_{sr}a_s - (\gamma_{sr+s} + i\Delta_{sr+s}(x))a_{sr+s} = 0 \qquad (4d)$$

where a_{0sd} is the amplitude of the second interaction beam, a_{1Br} is the near-backscatter transverse wave amplitude for the mutually resonant SBS driven by the primary interaction beam, a_{2Br} is the backscatter transverse wave amplitude for the mutually resonant SBS driven by the secondary interaction beam, and a_s represents other ion acoustic waves that can beat with a_{sr} to generate ion acoustic beat waves a_{sbr}. The coupling coefficients are given by

$$c_1 = d_1 = \frac{\omega_{pe}^2}{4\omega_0} \qquad c_2 = \frac{v_0^2\omega_0\omega_{s1}}{4v_e^2E_0^2(\omega_0 - \omega_{s1})} \qquad c_{2r} = c_2(\omega_{s1} \to \omega_{sr}) \qquad c_{b1} \approx \frac{\omega_{s1}}{2}$$

$$c_{s1+s} \approx \frac{\omega_{s1+s}}{2} \qquad c_{br} \approx \frac{\omega_{sbr}}{2} \qquad c_r \approx \frac{\omega_{sr}}{2} \qquad c_{LD+s} \approx \frac{\omega_{sLD+s}}{2} \qquad c_{LD} \approx \frac{\omega_{sLD}}{2}$$

$$d_2 = -\frac{k_{L1}^2v_0^2\omega_0\omega_{BG}}{4\omega_{pe}^2\omega_{1R}E_0^2} > 0 \quad d_3 = \frac{\omega_{pe}^2k_{L1}\omega_{L2}}{4\omega_{L1}k_{L2}\omega_{L1}} \qquad d_4 = -\frac{\omega_{pe}^2k_{L2}\omega_{L1}}{4\omega_{L2}k_{L1}\omega_{L2}} > 0$$

$$d_5 = \frac{\omega_{sLD}}{4k_{L1}^2\lambda_e^2(1+k_{sLD}^2\lambda_e^2)}\frac{k_{L1}\omega_{L2}}{k_{L2}\omega_{L1}} \qquad d_3d_4 \approx \frac{\omega_{pe}^2}{16} \qquad (5)$$

where γ's are temporal damping rates, $\Delta(x)$'s are spatially dependent mismatch frequencies, v_{gR}, v_{gB}, etc. are group velocities, and the IAW mode coupling coefficients have been evaluated in the fluid limit for $k^2\lambda_e^2 << 1$.[13] The mode amplitudes are defined with respect to the real electric field amplitudes for the electromagnetic waves and the amplitudes of the electron density perturbations for the Langmuir and ion acoustic waves:

$$a_0 = E_0(\omega_0) \quad a_{0sd} = E_{0sd}(\omega_0) \quad a_{1R} = E_{-R}^t(\omega_{1R} = \omega_{L1} - \omega_0) \quad a_{1B} = E_{-B}^t(\omega_{1B} = \omega_{s1} - \omega_0)$$

$$a_{2B} = E_{-B}^t(\omega_{2B} = \omega_{s2} - \omega_0) \quad a_{1Br} = E_{-B}^t(\omega_{1Br} = \omega_{sr} - \omega_0) \quad a_{2Br} = E_{-B}^t(\omega_{2Br} = \omega_{sr} - \omega_0)$$

$$a_{L1} = \frac{\delta n_{eL1}(\omega_{L1})}{n_{0e}} \qquad a_{L2} = \frac{\delta n_{eL2}(\omega_{L2} = \omega_{sLD} - \omega_{L1})}{n_{0e}} \qquad a_{sLD} = \frac{\delta n_{esLD}(\omega_{sLD})}{n_{0e}}$$

$$a_s = \frac{\delta n_{es}(\omega_s)}{n_{0e}} \quad a_{s1} = \frac{\delta n_{es1}(\omega_{s1})}{n_{0e}} \qquad a_{s2} = \ldots \qquad (6)$$

As diagrammed in the schematic in Fig. 6, we have included additional coupled mode equations for the SBS interaction of a secondary interaction beam and associated decay waves, and their coupling with the other ion waves in the system. In general, the ion acoustic beat waves are not linear normal modes; they are driven quasi-modes, and it is reasonable to treat them as being heavily damped. Only equations for the SRS and SBS decay waves are included in the system, and there is

no pump depletion allowed in this model unless the equation set were augmented by envelope equations for the pump wave amplitudes. Thus, the only nonlinearities retained that can influence SBS and SRS are secondary decay and ion wave mode coupling.[8,13,17] Pump depletion is analyzed in Sec. IV.

In considering SBS and SRS, our model omits particle trapping in the electron plasma waves[29] and ion acoustic waves.[13,17,30] However, trapping can be important. When is trapping relatively unimportant? In the presence of LDI, a rich spectrum of electron plasma waves arises that modifies the resonant kinetic response of the electrons and alters the simple picture of trapping in a single wave.[29] In the limit that the wave-particle correlation time becomes short compared to the trapping time, a fluid description for SRS and LDI sometimes can be justified.[9,21,31] Similarly, with multiple laser interaction beams and multiple SBS-driven ion acoustic waves we expect that the wave-particle correlation times for the ion waves will generally decrease compared to the trapping times in the waves, which will weaken the ion trapping effects. An exception to this is the mutually resonant SBS-driven ion wave excited by two laser interaction beams whose amplitude and ability to trap ions increase as the intensity is increased in the second laser beam. We note that the simulations of SBS with a secondary source of ion waves in Ref. 17 observed both ion trapping and ion wave mode coupling. As the second source of ion waves was increased in amplitude the ion wave mode coupling increased. To keep our model reasonably simple, we are omitting particle trapping.

From these coupled mode equations we recover the standard expressions for the growth rates for SBS and SRS backscatter, LDI, and the two-ion wave decay,[13,32] which can be viewed as a validity check on the system and illustrates the physics content of the system. In the sum over ion wave mode couplings in Eqs.(2b), (3b), and (4c), we can include IAW self-couplings to generate the second harmonic IAW which will provide a nonlinear shift of the IAW dispersion and dissipation proportional to the square of the local IAW amplitude.[13] However, we will primarily be concerned with the nonlinear effects due to the cross-coupling of two laser interaction beams and their principal IAW decay products. Equations (1-6) extend the equations set given in Refs. 8 and 17 by

including equations for SRS and LDI, and the SBS equations for the secondary laser interaction beam and mutually resonant SBS. In the next section we give the results of various analytical reductions of the coupled mode equations. We will also report the results of numerical integrations that illustrate the effects of the secondary nonlinear couplings in subsequent sections of the paper.

III. ANALYSIS OF PARAMETRIC INSTABILITIES AND REDUCTION OF COUPLED MODE EQUATIONS FOR LULI PLASMA CONDITIONS

In this section we obtain a number of analytical results for SBS, SRS, and LDI parametric instabilities and the modifications introduced by ion wave mode coupling. We evaluate parametric instability conditions for LULI laser-plasma experimental conditions and show that SBS, SRS, LDI, and self-focusing are likely to occur in intense speckles.

A. Analysis of Parametric Instabilities and Reduction of Coupled Mode Equations

From the algebraic reduction of Eqs.(1), (2), (5), and (6) we directly obtain the following expression for the local spatial growth rate of SRS backscatter in the limit that the damping of the backscattered Langmuir wave a_{L2} dominates its convection (our numerical integrations do not make this assumption):

$$\kappa_{SRS} = \mathrm{Re}\frac{1}{v_{gR}}\left(\frac{\gamma_{SRS}^2}{\gamma_{L1} + i\Delta_{L1} + \dfrac{\omega_{pe}^2 |\delta n_{esLD}/n_{0e}|^2}{16\gamma_{L2}}} - \gamma_{1R}\right) \qquad (7)$$

where the square of the SRS backscatter temporal growth rate is $\gamma_{SRS}^2 \approx [\omega_{pe}/(\omega_0 - \omega_{pe})]k_{L1}^2 v_0^2/16$ for $k_{L1}^2\lambda_e^2 << 1$, $v_0 = eE_0/m_e\omega_0$ is the electron quiver velocity in the primary interaction beam, and $\Delta_{L1} \approx \Delta_{L1}^0(x) + (\omega_{pe}^2/2)\delta n_e^{IAW}(x)/n_{0e}$ from n_{0e} and IAW detuning.[33] The result in Eq.(7) is the standard result[9,12] with the inclusion of the effect of the LDI on SRS deriving from the algebraic reduction of Eqs.(1a,b, and 2a). This illustrates that the LDI coupling provides an increase in the effective damping rate for the SRS EPW. The local value of the SRS-produced electron plasma wave (EPW) amplitude is concomitantly reduced by the LDI:

$$\frac{\delta n_{eL1}}{n_{0e}} = \frac{-ik_{L1}^2 v_0^2 \omega_0 E_{-R}^t / E_0}{4\omega_{pe}\left(\omega_0 - \omega_{pe}\right)\left(\gamma_{L1} + i\Delta_{L1} + \dfrac{\omega_{pe}^2 |\delta n_{esLD}/n_{0e}|^2}{16\gamma_{L2}}\right)} \tag{8}$$

and for purposes of estimates the scaling of the reflected SRS wave amplitude is given in terms of the SRS reflectivity R_{SRS} by $E_{-R}^t / E_0 \sim \sqrt{R_{SRS}}$. The results in Eqs.(7) and (8) illustrate the reduction in SRS effected by LDI. The observation that increased damping in the LDI decay product wave due to nonlinearities inhibits LDI and leads to an increase in the SRS gain has been made by other authors previously.[21,31,34]

For fixed EPW amplitude a_{L1} the LDI equations, Eqs.(2a) and (2b) yield the following local spatial growth rate for LDI electron plasma wave propagating in the backward direction

$$\kappa_{LDI} = -\mathrm{Re}\frac{d}{dx}\ln a_{L2} = \frac{1}{v_{gL2}}\left[\mathrm{Re}\frac{\gamma_{LDI}^2}{\gamma_{sLD} + i\Delta_{sLD} + \sum_s \dfrac{\omega_{sLD}\omega_{LD+s}|\delta n_{es}/n_{0e}|^2}{4\left(\gamma_{sLD+s} + i\Delta_{sLD+s}\right)}} - \gamma_{L2}\right] \tag{9}$$

where the square of the LDI temporal growth rate is $\gamma_{LDI}^2 = \frac{\omega_{pe}^2}{16}\frac{\omega_{sLD}}{\omega_{L1}-\omega_{sLD}}\frac{1}{1+k_{sLD}^2\lambda_e^2}\left|\frac{\omega_{L1}}{k_{L1}v_e}\frac{\delta n_{e,L1}}{n_{0e}}\right|^2$ and $v_{gL2} = 3k_{L2}\lambda_e^2 v_e$. The nonlinearity due to second harmonic generation of the LDI IAW corresponds to setting the coupling IAW equal to the LDI IAW, i.e., $s = sLD$ in the summation over ion waves in Eq.(9). The spatial growth rate for LDI EPW decay wave and the amplitude of the decay IAW decay wave are reduced by the coupling to other sound waves:

$$\frac{\delta n_{esLD}}{n_{0e}} = \frac{-i\omega_{sLD}}{4\left(1+k_{sLD}^2\lambda_e^2\right)}\frac{\left(\delta n_{eL1}/n_{0e}\right)\left(\delta n_{eL2}^*/n_{0e}\right)}{\left(\gamma_{sLD} + i\Delta_{sLD} + \sum_s \dfrac{\omega_{sLD}\omega_{LD+s}|\delta n_{es}/n_{0e}|^2}{4\left(\gamma_{sLD+s} + i\Delta_{sLD+s}\right)}\right)} \tag{10}$$

The results of Eqs.(7-10) indicate that the IAW mode coupling reduces the sound wave amplitude δn_{esLD} in LDI, which in turn increases δn_{eL1} and the local SRS spatial growth rate in Eqs.(7) and (8).

The local spatial growth rate for SBS backscatter obtained from Eqs.(3-6) is also reduced by IAW mode coupling:

$$\kappa_{SBS} = -\mathrm{Re}\frac{d}{dx}\ln a_{1B} = \frac{1}{v_{gB}}\mathrm{Re}\left(\frac{\gamma_{SBS}^2}{\gamma_{s1} + i\Delta_{s1} + \sum_s \frac{\omega_{s1}\omega_{s1+s}\,|\,\delta n_{es}/n_{0e}\,|^2}{4(\gamma_{s1+s} + i\Delta_{s1+s})}} - \gamma_{1B}\right) \tag{11}$$

where $\gamma_{SBS}^2 = \frac{\omega_{s1}\omega_{pe}^2}{\omega_0 - \omega_s}\frac{v_0^2}{16v_e^2}$ is the temporal growth rate for Brillouin backscatter. The harmonic generation IAW nonlinearity corresponds to $s = s1$ in Eq.(11). The SBS IAW amplitude is given by:

$$\frac{\delta n_{es1}}{n_{0e}} = \frac{-i\omega_{s1}(v_0^2/4v_e^2)(E_{-B}^t/E_0)}{\gamma_{s1} + i\Delta_{s1} + \sum_s \frac{\omega_{s1}\omega_{s1+s}\,|\,\delta n_{es}/n_{0e}\,|^2}{4(\gamma_{s1+s} + i\Delta_{s1+s})}} \tag{12}$$

where $E_{-B}^t/E_0 \sim \sqrt{R_{SBS}}$ and R_{SBS} is the reflected SBS power fraction for purposes of estimates and scaling arguments. Thus, ion wave mode coupling can decrease SBS while increasing SRS if the processes overlap.

The results obtained in the preceding equations indicate that mode coupling and harmonic generation can be viewed as producing a nonlinear increase in the dissipation of a driven wave and a nonlinear shift of the effective resonant frequency. The nonuniformity of the nonlinear increase in dissipation is significant. Consider the convective gain for SRS backscatter in a nonuniform plasma in the absence of linear damping of the backscattered transverse wave:

$$-\frac{d\ell nE_{-R}^t}{dx} = \kappa_{SRS} = \mathrm{Re}\frac{\gamma_{SRS}^2}{v_{gR}(\gamma_{L1}(x) + i\Delta_{L1}(x))} \tag{13}$$

Integrate across the domain to obtain the gain exponent:

$$G_{SRS} = \int dx\kappa_{SRS}(x) = \int dx\frac{\gamma_{SRS}^2}{v_{gR}}\frac{\gamma_{L1}}{\gamma_{L1}^2 + \Delta_{L1}^2} \tag{14}$$

where $\Delta_{L1} = \omega_{pe}x/2L_{ne}$. With spatially constant damping γ_{L1} and the nonuniformity of the integrand dominated by the linear variation in x of Δ_{L1} through the resonance at x=0, the Rosenbluth result[35,36] is recovered that the gain exponent is *independent* of damping in a *linear* gradient:

$$G_{SRS}^0 = 2\pi L_{ne}\gamma_{SRS}^2/v_{gR}\omega_{pe} \tag{15}$$

If the damping of the primary decay EPW in SRS (or the IAW in SBS) is nonlinearly enhanced where the decay product waves are big, e.g., for $x < 0$ relative to the resonance at $x = 0$, then there can be a reduction in the gain exponent by up to ~1/2 in this simplest of models:

$$G_{SRS} \rightarrow \left\{1 + \frac{1}{\pi}\left[-\tan^{-1} 4 + \tan^{-1}\left(4\gamma_{L1}/\gamma_{nl}\right)\right]\right\} G^0_{SRS} \qquad (16)$$

for $\gamma_L=\gamma_{nl}>\gamma_{L1}$ over $-4x_r \le x \le 0$ and $\gamma_L=\gamma_{L1}$ elsewhere, where x_r=the resonance width=$(2\gamma_{L1}/\omega_{pe})L_{ne}$. In actuality the nonlinear damping has a more complicated spatial dependence than in this model. Nevertheless, this simple model suffices to demonstrate that if LDI and IAW mode coupling produce enhanced damping in the SRS and SBS active regions, this will lead to gain reductions.

B. Parametric Instabilities for LULI Plasmas Condtions

The LULI experimental conditions have been described in several publications.[1-7] A six laser beam facility was used with three heater beams at 0.53 μm with random phase plates (RPP) to produce and heat an underdense plasma from a CH foil. Two or three *f*/6 laser interaction beams at 1.053 μm also with random phase plates (RPP) were used to study laser plasma interactions making relative angles 22.5˚, 45˚, and 67.5˚. Thomson scattering with a probe beam at 0.35 μm has been used to identify the plasma waves associated with parametric instabilities. The maximum electron density on the laser axis varied between 0.3 n_c and 0.08 n_c, where n_c is the critical density for 1.053 μm. Nominal LULI parameters in CH foils at a nominal reference time (~2 ns in the LASNEX[37] simulation shown in Fig. 7) near the peak of the plasma are: n_e/n_c=0.1, T_e/T_i~2.4, T_e=0.5keV, density scale length $L_{ne}=n_e/|dn_e/dx|$~500-1000μm, plasma flow velocity scale length $L_V=c_s/|dV/dx|$~300μm, speckle length~300μm, I_0~10^{14} W/cm^2, <Z>=3.5 for CH. The damping rates for the SBS ion waves (set by ion Landau damping) and the SRS electron plasma waves (set dominantly by electron-ion collisions for $2k_0\lambda_e$=0.2) are γ_s/ω_s=~0.1 and $\gamma_{EPW}/\omega_{pe}=\nu_{ei}/(2\omega_{pe})$~0.001 where ν_{ei} the electron-ion angular scattering rate, $\nu_{ei}=(\langle Z^2\rangle/\langle Z\rangle)\nu_{ee}, \nu_{ee}=2.91\times10^{-6}s^{-1}n_e(cm^{-3})\ell n\Lambda/T_e(eV)^{3/2}$, <$Z^2$>=13.5, and <$Z$>=3.5 where Z is the ionic charge state.

Local thresholds for SBS and SRS are satisfied at the average intensity I_0 of the primary interaction beam at the peak of the primary interaction beam pulse and at the nominal reference plasma density (of course, the thresholds depend in detail on the laser pulse profile in time and space, and the plasma density and temperature profiles in time and space which evolve as depicted in the LASNEX simulation shown in Fig. 7). The local SRS backscatter threshold[12] is set by collisional damping of the backscattered electromagnetic wave and the decay electron plasma wave (the electron Landau damping of the EPW is much weaker than its collisional damping):

$$\gamma_{SRS} = \left(\frac{\omega_{pe}}{\omega_0 - \omega_{pe}}\right)^{1/2} \frac{k_{L1} v_0}{4} \sim 5.1 \times 10^{12} s^{-1} (I/I_0)^{1/2} > (n/n_c)^{1/2} (\nu_{ei}/2) \sim 5 \times 10^{11} s^{-1} \qquad (17)$$

where γ_{SRS} is the local SRS backscatter temporal growth rate. The local SBS backscatter threshold is set by collisional damping of the backscattered electromagnetic wave and the Landau damping of the decay ion wave:

$$\gamma_{SBS} = \left(\frac{\omega_s \omega_{pe}^2}{\omega_0 - \omega_s}\right)^{1/2} \frac{v_0}{4 v_e} \sim 1.2 \times 10^{12} s^{-1} (I/I_0)^{1/2} > (n/n_c)^{1/2} (\nu_{ei}/2)^{1/2} \gamma_s^{1/2} \sim 10^{11} s^{-1} \qquad (18)$$

where γ_{SBS} is the local SBS backscatter temporal growth rate.

The LULI experimental observations[1-4,6-7] showed that SBS occurred before SRS did in time. The peak SBS signals originated from farther out in the plasma (an nearer the incident laser) than did the SRS signals, and the latter did not originate from the peak of the density profile where the original foil's location was. The Rosenbluth convective gains for SRS and SBS in a linearly inhomogeneous plasma are significant in speckles for LULI parameters. The Rosenbluth convective gain exponent[35] for the electric field amplitude in SRS backscatter for the reference LULI parameters is

$$G_{SRS}^0 = \frac{\pi \gamma_{SRS}^2}{\Delta k' v_1 v_2} = \frac{\pi}{8} \frac{\omega_0 L_{ne}}{k_0 c^2} \frac{\omega_{pe}^2}{\omega_0 - \omega_{pe}} k_{L1}^2 \lambda_e^2 \sim (I/10^{14} W/cm^2)(L_{ne}/1000\,\mu m) \rightarrow \sim 4 \text{ at } I = 4 I_0 \qquad (19)$$

where $v_1 = k_0 c^2/\omega_0$, $v_2 = 3k\lambda_e v_e$, and $\Delta k'/k \sim 1/6 k^2 \lambda_e^2 L_{ne}$, i.e., the SRS gain is limited by the linear electron density inhomogeneity away from the peak of the plasma density (see Fig. 7). The corresponding gain exponent for SBS backscatter is[23]

$$G^0_{SBS} = \frac{\pi\gamma^2_{SBS}}{\Delta k' v_1 v_2} = \frac{\pi}{16}\frac{\omega^2_{pe}}{\omega_0 - \omega_s}\frac{\omega_0 L_V}{k_0 c^2}\frac{v_0^2}{v_e^2} \sim 2.5(I/10^{14} W/cm^2)(L_V/300\,\mu m) \rightarrow \sim 10 \text{ at } I = 4I_0 \quad (20)$$

where $v_1 = k_0 c^2/\omega_0$, $v_2 = c_s$, and $\Delta k'/k \sim 1/L_V$, i.e., the SBS gain is limited by the linear flow velocity gradient. The velocity gradient is weaker as one moves out from the peak density, but the plasma density also decreases which weakens the local SBS growth rate and the gain (Fig. 7). In addition, there is the spatial dependence of the laser beam intensity to take into account. Thus, the spatial dependence of the quasi-local SBS convective gain is not simple. Nevertheless it is clear from Eq.(20) that only the more intense speckles in the interaction beam lead to significant SBS reflectivity as was concluded in earlier work.[23]

If the electron density profile at its peak is a smooth parabola, then SRS may satisfy conditions for absolute instability, e.g.,[38]

$$\frac{2\pi\gamma^2_{SRS}}{|\Delta k''|^{2/3}|v_1 v_2|} \sim 16(I/10^{14} W/cm^2)(L_{ne}/300\,\mu m)^{4/3} > 1 \quad (21)$$

where $v_1 = c$, $v_2 = 3k\lambda_e v_e$, $|\Delta k''| = (1/6k\lambda_e)(1/\lambda_e L_{ne}^2)$ for $\Delta k' = 0$, and L_{ne} is the parabolic density scale length**.** In fact, SRS backscatter may have to be absolutely unstable in order to account for the observed LULI reflectivities because the linear convective gains are too weak. However, the plasma is not perfectly smooth, which alters the consideration of the SRS absolute instability near the peak of the density profile.[39]

We conclude that the SBS convective gain exponents are bigger than the SRS convective gains away from the peak of the plasma. Thus, with SBS observed to occur farther out in the plasma, pump depletion in the most intense speckles (which are the most active for SRS and SBS) due to SBS can account for why SRS (either absolute or convective) is not observed in the same speckle until SBS quenches.[2]

Another consideration for LULI plasma conditions is whether ponderomotive and thermal filamentation can occur. The linear convective gain for the growth of electron density perturbations in ponderomotive filamentation over a 300μm speckle is significant:[9-12,40]

$$\mathrm{Im}\, k_{\|} L \sim \frac{k_0 L}{8} \frac{n}{n_c} \frac{v_0^2}{v_e^2} \sim 1.5 \frac{I}{I_0} \tag{22}$$

Thermal self-focusing[8-12,40] (for CH, <Z>=3.5, and $ZT_e/T_i >> 1$) is even stronger:

$$\mathrm{Im}\, k_{\|} L \sim \frac{k_0 L}{(k_0 \ell_s)^{2/3}} (v_0/v_e)^{4/3} (n/n_c)^{2/3} \sim O(4)(I/I_0)^{2/3} \tag{23}$$

where ℓ_s is the energy loss mean-free-path defined in Eq.(77) of Kaiser *et al.*,[40]

$$\ell_s = \frac{4}{3}\sqrt{\frac{1}{3\pi}\frac{Z^2}{Z+1}}\ell_e \sim O(1)\ell_e \sim \frac{v_e}{\nu_{ei}} \sim 10^{-3} cm \tag{24}$$

The significant likelihood of filamentation and self-focusing motivates using a filamented speckle intensity probability distribution function in addition to a normal (unfilamented) RPP distribution in calculations introduced later in this paper.

The local threshold for Langmuir Decay Instability is set by collisional damping of the decay product (backscattered) EPW and the ion Landau damping of the ion wave for LULI conditions:

$$\gamma_{LDI}^2 \geq \gamma_{L2}\gamma_s \sim (\nu_{ei}/2)\gamma_s \quad \rightarrow \left|\delta n_{eL1}/n_{0e}\right|^2 \geq 16 k_{L1}^2 \lambda_e^2 (\nu_{ei}/2\omega_{pe})(\gamma_s/\omega_s) \tag{25}$$

For LULI conditions $k_{L1}\lambda_e \sim 0.16$ and $|\delta n_{eL1}/n_{0e}| > 0.007$ for LDI to occur. An estimate of the local amplitude of a damped EPW driven by SRS at resonance is readily obtained from the SRS coupled mode equations:

$$\frac{\delta n_{eL1}}{n_{0e}} = \frac{-ik_{L1}^2 v_0^2 \omega_0 E_{-R}^t / E_0}{4\omega_{pe}(\omega_0 - \omega_{pe})\gamma_{L1}} \sim \frac{-ik_{L1}^2 v_0^2 \omega_0 \sqrt{R_{SRS}}}{4\omega_{pe}(\omega_0 - \omega_{pe})\gamma_{L1}} \tag{26}$$

For LULI conditions, $|\delta n_{eL1}/n_{0e}| \sim (I/I_0)\sqrt{R_{SRS}}$, e.g., $|\delta n_{eL1}/n_{0e}| \sim 0.1(I/I_0)$ for $R_{SRS} \sim 0.01$, which is well above the LDI local threshold for $I \geq I_0$. The LDI EPW has been observed with Thomson scattering in LULI experiments.[5] For LDI to have much influence in saturating SRS, the damping enhancement due to LDI in Eq.(9) must be comparable to the linear damping of the primary SRS EPW:

$$\frac{\omega_{pe}^2 |\delta n_{esLD}/n_{0e}|^2}{16\gamma_{L2}} \geq \gamma_{L1} \rightarrow |\delta n_{esLD}/n_{0e}| \geq 4\sqrt{\gamma_{L1}\gamma_{L2}/\omega_{pe}^2} \sim 0.004 \tag{27}$$

Because the EPW damping rates (if the electron distribution is a Maxwellian) are relatively weak (set by collisions), LDI has a low threshold and can affect SRS at relatively small amplitude of the LDI decay-product ion wave.

The beating of the SBS ion wave with the SRS EPW (if the two overlap in space and time, and both are driven to large amplitude) leads to an effective increase in the dissipation of the SRS EPW that is qualitatively similar to that produced by the LDI ion wave and the reduction it produces in both the SRS convective growth rate and the SRS EPW amplitude.[41] In LULI conditions, if the SRS backscatter-produced EPW can beat with the SBS backscatter-produced IAW, the resulting forward scattered EPW will have a value of $k\lambda_e \sim 0.35$ giving rise to a linear dissipation rate $\sim 0.05\omega_{pe}$ which is significantly higher than the dissipation rate of the SRS EPW and there is a significant mismatch frequency for the three-wave resonance, $\sim 15k_0^2\lambda_e^2\omega_{pe} \sim 0.15\omega_{pe}$, both of which will strongly limit the amplitude of the beat-wave EPW. There is also a backward traveling EPW beat wave with wavenumber $-0.3k_0$. The damping of this wave is very weak for the LULI parameters, just the collisional damping, but the three-wave mismatch frequency is approximately $4k_0^2\lambda_e^2\omega_{pe} = 0.04\omega_{pe}$ which is much bigger than the damping rate of the SRS EPW and will limit the amplitude of the backward propagating EPW beat wave.

Using the mode coupling equations derived here, we can estimate the effects of the SBS ion wave beating with the SRS EPW. The coupling of the SBS ion wave to the two EPW beat waves contributes two additional additive terms in the denominator of κ_{SRS} in Eq.(7) and similarly in Eq.(8) for $|\delta n_{eL1}/n_{0e}|$, the SRS EPW amplitude, so that the relevant term in the denominator becomes:

$$\gamma_{L1} + i\Delta_{L1} + \frac{\omega_{pe}^2 |\delta n_{esLD}/n_{0e}|^2}{16\gamma_{L2}} + \sum_{i=1,2} \frac{\omega_{pe}^2 |\delta n_{es1}/n_{0e}|^2}{16(\gamma_{LB,i} + i\Delta_{LB,i})} \qquad (28)$$

where the sum is over the two EPW beat waves, and $\gamma_{LB,i}$ and $\Delta_{LB,i}$ are the damping rate and frequency mismatch of the EPW beat waves, respectively. From Eq.(28) we derive a condition on the magnitude of the SBS IAW needed to contribute to the reduction of the SRS EPW amplitude and the SRS gain rate:

$$|\delta n_{es1}/n_{0e}|^2 \geq 16\gamma_{L1} \left| \sum_{i=1,2} \omega_{pe}^2 / (\gamma_{LB,i} + i\Delta_{LB,i}) \right|^{-1} \qquad (29)$$

For the LULI parameters described, $|\delta n_{es1}/n_{0e}| \geq 0.02$ for the coupling of SBS to the two EPW beat waves to contribute additional dissipation and mismatch comparable to the SRS EPW linear

damping rate, which increases the threshold for SRS and decreases its gain. We note that the SRS saturation mechanism afforded by LDI becomes significant for an IAW relative amplitude a factor of 5 smaller in Eq.(27) than here in Eq.(29) because LDI involves three waves much closer to linear resonance and the LDI scattered EPW is very weakly damped.

In general, the coupling of the SBS IAW and the SRS EPW will also have a back-reaction on the SBS IAW which we can estimate from the mode coupling equations. The scattering of the SRS EPW into a forward-scattered EPW with more than twice the original EPW wavenumber increases the effective damping for both the SRS EPW and the SBS IAW, while the backscattered EPW at small wavenumber and the SBS IAW grow at the expense of the SRS EPW. By including equations for the driven EPW beat waves similar to Eq.(2a), whose solutions are substituted into two new terms in Eq.(3b) driving a_{s1} of the same form as the term $id_5 a_{L1} a_{L2}$ (but with the EPW beat-wave amplitudes $a_{LB,1}$ or $a_{LB,2}$ replacing a_{L2}), we obtain the additional source term in the right side of Eq.(3b):

$$\sum_{i=1,2} \frac{d_{4,i} d_{5,i} |\delta n_{L1} / n_{0e}|^2}{(\gamma_{LB,i} + i\Delta_{LB,i})} \rightarrow \sum_{i=1,2} \frac{(-1)^{i-1} \omega_{pe} |\delta n_{L1} / n_{0e}|^2}{16 k_{L1}^2 \lambda_e^2 (\gamma_{LB,i} + i\Delta_{LB,i})} \omega_{s1} a_{s1} \qquad (30)$$

For $|\delta n_{eL1} / n_{0e}| \approx 0.01$ just above the local LDI threshold calculated from Eq.(25), the magnitude of the additional drive term due to the EPW beat waves given in Eq.(30) is $<5\times10^{-3}\omega_{s1}a_{s1}$, which is more than an order of magnitude smaller than the linear dissipation term $-\gamma_1 a_{s1}$ in Eq.(3b).

For ion wave mode coupling to have much influence in saturating SBS or in reducing the LDI IAW amplitude which in turn renders LDI less effective in saturating SRS, the enhanced damping due to IAW mode coupling in Eq.(11) must be comparable to the linear damping at resonance for SBS in a speckle:

$$\sum_s \frac{\omega_{s1}\omega_{s1+s} |\delta n_{es} / n_{0e}|^2}{4(\gamma_{s1+s} + i\Delta_{s1+s})} \geq \gamma_{s1} \rightarrow |\delta n_{es} / n_{0e}| \geq 2\sqrt{|(\gamma_{s1+s} + i\Delta_{s1+s})\gamma_{s1}|/(\omega_{s1+s}\omega_{s1})} \sim 0.2 \quad (31)$$

for the LULI reference conditions, where $\gamma_s / \omega_s \approx 0.1 >> |\Delta_s / \omega_s| \sim k_s^2 \lambda_e^2 / 2 \sim 0.02$. IAW amplitudes driven by SBS at resonance can be sufficiently large locally to satisfy the condition in

Eq.(31):

$$\frac{\delta n_{es1}}{n_{0e}} = \frac{-i\omega_{s1}(v_0^2/4v_e^2)(E_B^t/E_0)}{\gamma_{s1}} \sim \frac{-i\omega_{s1}(v_0^2/4v_e^2)\sqrt{R_{SBS}}}{\gamma_{s1}} \qquad (32)$$

For the LULI reference conditions, $|\delta n_{es1}/n_{0e}| \sim 0.2(I/I_0)\sqrt{R_{SBS}}$; and $|\delta n_{es1}/n_{0e}| \sim 0.2$ for $R_{SBS} \sim 0.01$ in a $I=5I_0$ speckle at SBS resonance. These results suggest that multiple SBS-active beams in LULI can induce IAW mode coupling that can reduce SBS, reduce LDI and enhance SRS in consequence. We should also note that the condition for significant ion wave mode coupling in Eq.(31), if only one ion wave dominates the sum over waves, is much the same as the threshold condition for the two-ion wave decay[13,32] in which an ion wave decays to two daughter waves at longer wavelengths. Thus, in the limit that ion wave mode coupling is significant, we expect other manifestations of ion wave turbulence.

Our treatment of SRS backscatter and LDI only considers the first LDI step. The SRS and LDI phenomena is much richer than what can be incorporated here.[31] Recent studies of LDI and SRS examine in various degrees of detail multiple LDI cascade steps or collapse of the electron plasma wave spectrum depending on how short the EPW wavelength is compared to the Debye length.[31] In contrast, we have terminated our calculations at the first LDI step but have included ion wave coupling between the SBS and SRS + LDI phenomena. We have already shown that IAW mode coupling inhibits LDI, which in turn weakens the saturation of SRS by LDI. The inhibition of the first LDI step also make less energy available to drive a cascade or collapse. In addition, any other scattering of EPWs in the spectrum of ion waves should be similarly inhibited by the increased IAW damping due to the mode coupling that inhibits the first LDI step.

C. Numerical Solution of the Coupled Mode Equations for SRS, SBS, and LDI

To study the interaction of SBS, SRS, LDI, and ion wave mode coupling in more generality and more quantitatively, we have numerically integrated the coupled mode equations Eqs.(1-6) in steady state. These are a set of first-order differential equations in the one spatial variable x (direction normal to the foil and parallel to the primary interaction beam) with nonlinear coupling terms as sources. We used a finite-difference representation of the spatial derivatives and iterated on the source terms to approximately center them relative to the derivative terms so that the scheme was

second-order accurate and quite fast. The number of computational cells employed was 10^4 to resolve the domain, whose length was set equal to a speckle length, 300 μm. With the interaction beams incident from the left, the integration proceeded from boundary conditions specifying thermal noise[9,23,42] at the right end of the plasma and swept to the left side of the domain where the reflected SRS and SBS signals were monitored. The evaluation of the thermal noise for the backscattered electromagnetic waves and the backscattered EPW in LDI is predicated on the validity of applying the fluctuation-dissipation theorem, knowledge of the electron and ion velocity distribution functions,[42] and a reasonable estimate for the volume in wavenumber space.[9] Thus, the evaluation leads to the following estimates:
$10^{-7} \le \left|E^t_{-R} / E_0\right|, \left|E^t_{-B} / E_0\right|, \left|\delta n_{eL2} / n_{e0}\right| \le 10^{-5}$ for the noise fields where E_0 corresponds to $I_0=10^{-14}$ W/cm^2 incident power. We have used 10^{-5} and 10^{-6} for the boundary values representing noise at the right side boundary of the domain for the dimensionless relative amplitudes of the backscattered transverse waves and the LDI EPW decay wave, respectively.

In the event that the relative electron density perturbation in a mode or the reflectivity in a backscattered transverse wave exceeded unity in magnitude, the numerical calculation saturated the electron density perturbation or the reflectivity at unity in magnitude while retaining the computed phase (when this occurs the validity of the model is breaking down). Other nonlinearities should come into play if the relative density perturbation approaches unity or if the reflectivity is approaching unity. In the results reported here, the relative perturbed electron density never approached unity. However, the reflectivity did approach unity very near the left boundary in a few of the SBS and SRS cases, which indicated that pump depletion effects should have been retained in those few cases.

As a check of the numerical integration of the coupled mode equations we first integrated the SBS equations for various choices of the product of the primary laser beam intensity and the plasma flow velocity gradient using the reference LULI parameters with SRS and LDI suppressed (Fig. 8). The results for the fractional SBS power reflected R_{SBS} agree well with the Rosenbluth

linear convective gain in the linear regime. Similarly good agreement with the Rosenbluth linear convective gain has been obtained for SRS with SBS and LDI suppressed (Fig. 9).

IV. PUMP DEPLETION EFFECTS

A. Solutions of Coupled Mode Equations Based on Action Conservation

The coupled mode equations in Sec. II describing the parametric instabilities omit the equations for the pump wave propagation and pump depletion. By including equations for the pump wave ampitudes in the SRS and SBS equations analogous to Eqs.(1a) and (3a) for the backscattered transverse waves and introducing the wave action flux densities,[36] $J_\ell = (m_e c^2/e)^2 (k_\ell/8\pi)|u_\ell/c|^2$ where $u_\ell = -ieE_\ell/m_e\omega_\ell$ and $E_\ell(\mathbf{x},t) \equiv (1/2)E_\ell \exp(-i\omega t + i\mathbf{k}\ \mathbf{x}) + c.c.$, the coupled mode equations for SRS or SBS backscatter for a single interaction beam including pump depletion can be written in terms of the wave action (from which the wave action flux conservation relations immediately follow[36]):

$$\frac{d}{dx} J_0 = \frac{d}{dx} J_1 = \alpha J_0 J_1 |\chi_e| \mathrm{Im}\, \varepsilon^{-1} \tag{33}$$

for weak damping relative to the wave frequencies, where (0,1) subscripts represent the pump and backscattered transverse waves, $\alpha = 2\pi[(\mathbf{k}_0 + \mathbf{k}_1)^2/k_0 k_1]|1 + \sum \chi_i|$, $\chi_{e,i}$ are the linear dielectric susceptibilities for electron and ion species, and $\varepsilon = 1 + \chi_e + \sum \chi_i$ is the linear longitudinal plasma dielectric function. Equation (33) describes either SRS or SBS backscatter with appropriate evaluation of $\chi_{e,i}$. In this equation, collisional damping of the transverse waves through the resonance zone of the three-wave interaction has been ignored.

For a plasma with spatial inhomogeneity varying linearly through the resonance $\mathrm{Re}\,\varepsilon = 0$, integration of Eq.(33) using the constancy of J_0-J_1 yields the generalized Tang formula for action transfer and pump depletion:[36,43]

$$(1-R)(1+R/\rho) = \exp[G_0(1-R-\rho)] \rightarrow G_0 = (1-R-\rho)^{-1} \ln[(1-R)(1+R/\rho)] \tag{34}$$

where $R = \Delta J/J_0$ the reflected action transfer fraction, $\rho = J_1^{in}/J_0^{in}$, and $G_0 = (\alpha/8)k_0 L|u_0/c|^2$ the Rosenbluth convective gain exponent for power, and $L = \left|\chi_e (d\varepsilon/dx)^{-1}\right| = \left|\chi_e \int_{-\infty}^{\infty} dx\ \mathrm{Im}\,\varepsilon^{-1}/\pi\right|$ at resonance ($L = L_v/2$ for SBS and $L = L_{ne}$ for SRS. For SBS in the LULI reference conditions, $G_0 = 5(I/10^{14} W/cm^2)(L_v/300\,\mu m)$, while for SRS

$G_0 = 1.4(I/10^{14} W/cm^2)(L_{ne}/1000\,\mu m)$. The solutions of Eq.(33) for R as a function of G_0 and ρ are given in Fig. 2 of Ref. 36.

With two interaction beams making a 22.5˚ relative angle with respect to one another, the mutually resonant IAW or EPW bisecting the two laser propagation directions can backscatter each of the incident beams back along the other interaction beam's path. Equation (33) becomes

$$\frac{d}{dx} J_{01} = \frac{d}{dx} J_1 = \alpha J_1 (J_{01} + J_{02}) |\chi_e| \operatorname{Im} \varepsilon^{-1} \quad (35a)$$

$$\frac{d}{dx} J_{02} = \frac{d}{dx} J_2 = \alpha J_2 (J_{01} + J_{02}) |\chi_e| \operatorname{Im} \varepsilon^{-1} \quad (35b)$$

where J_1 and J_2 are the action flux densities for the two nearly backscattered transverse waves issuing from J_{01} and J_{02}, respectively, which are the incident action flux densities of the two interaction beams. The direct backscatter of each of the two interaction beams produces independent ion waves and is *not* described by Eqs.(35a) and (35b). The solutions to these equations obtained by integrating across the resonance and using the constancy of J_{01}-J_1 and J_{02}-J_2 are

$$(1 - R_t)(1 + R_{1,2}/\rho_{1,2}) = \exp[G_t(1 - R_t - \rho_t)] \quad (36)$$

where $\rho_{1,2} = J^{in}_{1,2}/J^{in}_{01,02}$, $R_{1,2} = \Delta J_{1,2}/J^{in}_{01,02}$, $\rho_t = (J^{in}_1 + J^{in}_2)/(J^{in}_{01} + J^{in}_{02})$, and $G_t = (\alpha/8) k_0 L (|u_{01}/c|^2 + |u_{02}/c|^2)$. Equation (33) represents two equations for R_1 and R_2. For the special case of the second interaction beam much weaker than the primary, $J_{02} << J_{01}$, and $\rho_1 = \rho_2$, then $\rho_t \approx \rho_1$, $R_1 = R_2$, $R_t \approx R_1$, and

$$(1 - R_1)(1 + R_1/\rho_1) = \exp[G_t(1 - R_1 - \rho_1)] \rightarrow G_t = (1 - R_1 - \rho_1)^{-1} \ln[(1 - R_1)(1 + R_1/\rho_1)] \quad (37)$$

where $G_t = 6(L_v/300\,\mu m)(I^{in}_{01} + I^{in}_{02})/10^{14} W/cm^2$ for mutually resonant SBS and the reference LULI parameters. Note that Eq.(37) differs from Eq.(31) only in the replacement of the gain parameter G_t which is now proportional to the sum of the two interaction beam intensities and drives the mutually resonant SBS process more strongly in consequence. A plot of the reflectivity R_1 as a function of G_t for ρ_1=10^{-10} is given in Fig. 10. Thus, overlapping speckles from the two interaction laser beams with combined intensities in excess of 3-4 ×10^{14} W/cm^2 are needed to induce significant local pump depletion in both speckles. LULI observations[6] indicated strongly

enhanced signals for the mutually resonant SBS IAW when there were two interaction beams at finite amplitude.

B. Pump Depletion Effects Averaged Over the Speckle Intensity Distribution

In the preceding we have determined the backscatter reflectivity and pump depletion as a function of laser beam intensity for a single beam (direct backscatter) and for the mutually resonant near backscatter of two interaction beams. The laser beam in experiments is highly nonuniform, and higher intensity speckles will produce more backscatter locally. To obtain a beam-averaged estimate of the backscatter we need to take into account the speckle intensity distribution. A random phase plate (RPP) laser beam has an approximately exponential probability distribution function (PDF) of speckle intensities.[44] We have adopted the following "normal" PDF for an RPP beam: by $P_N(I)= \exp(-I/I_0)/I_0$. We also consider a second laser speckle intensity distribution with a more filamentary structure that has a more extended tail at high intensities. Motivated by F3D simulations,[14] we have modeled a "filamented" beam with $P_F(I)= a \exp(-I/0.5I_0)$ for $I \le 1.4I_0$, $P_F(I)= b \exp(-I/2I_0)$ for $I \ge 1.4I_0$ ($I_0=10^{14}$W/cm^2 for LULI) appropriately normalized and continuous at $1.4I_0$ (to determine a and b). The normal and filamented PDFs are plotted in Fig. 11.

Given a model for the PDF of the speckle intensity, we can average the reflectivity expressions obtained in Eqs.(34) and (37) over the speckle intensity distributions of the laser beams. The averaging of the exponential gain including saturation by pump depletion over the speckle intensity distribution to obtain a finite average reflectivity in the manner indicated is in the spirit of Ref. 45. To accomplish this average, we have inverted the relation between G_t and R_1 in Eq.(37) numerically to obtain R_1 as a function of G_t and then integrated R_1 with respect to both I_1 and I_2 weighted by the PDFs for I_1 and I_2, which result is plotted as a function of the average intensity of the second interaction beam $\langle I_2 \rangle$ in Fig. 12 for $\langle I_1 \rangle = I_0$. To a good approximation (because $\cos 11.25^\circ = 0.98 \sim 1$), the single-beam reflectivity for direct backscatter is recovered from the limit of R_1 as $\langle I_2 \rangle \rightarrow 0$ in Fig. 12. The overall expected pump depletion from the mutually resonant IAW is finite for LULI parameters (~1-3%), but not large, and is a slowly increasing function of the second beam

intensity. The filamented laser beams produce significantly more backscatter in this model. We should keep in mind that the local pump depletion is much higher in intense speckles ($I > 3\text{-}4\, I_0$) of the primary beam (or in the combination of the two interaction beams) than for the beam average.

We caution that if nonlinear filamentation and self-focusing are active (which we believe is the case in LULI intense speckles), then there will be a local depression of the electron density in intense speckles accompanying the local increase in laser intensity due to self-focusing. This effect has been neglected in our quasi-one-dimensional mode coupling model. Russell, DuBois, and Rose[31] showed that including or excluding the electron density perturbation due to self-focusing waves in their two-dimensional simulations significantly reduced the SRS backscatter in an initially uniform plasma due to detuning of the electron plasma wave or increased the SRS backscatter when only the laser intensity enhancement due to self-focusing was retained, respectively. Some of the fluid simulations of the competition of SRS and SBS reported in the Ref. 9 also observed a decrease in the SRS backscatter reflectivity at high laser intensities due to self-focusing produced density perturbations. However, in other simulations reported in Ref. 9 the SRS backscatter reflectivity was observed to increase due to self-focusing at lower laser intensities and at times before the density perturbations due to the self-focusing had a chance to grow to significant amplitudes. Thus, whether self-focusing increases or decreases SRS backscatter reflectivity depends in some detail on the circumstances and when the observations are made. Because our simplified model omits density detuning due to self-focusing, this question is moot. In an inhomogeneous plasma when both SBS and self-focusing are active, the work of Tikhonchuk, Huller, and Mounaix[46] has shown that SBS backscatter reflecitivity can be enhanced significantly near the threshold power for self-focusing; and at higher powers pump depletion due to SBS in a single speckle may inhibit significant self-focusing from occurring. Use of the filamented speckle intensity distribution in our modeling captures the former enhancement effect. In any case, the consideration of the alternative filamented speckle intensity distribution is useful because it allows us to examine the sensitivity of the results to the kind of speckle intensity distribution assumed.

C. Inhibition of Primary Backscatter by Pump Depletion from Two-Beam Near-Backscatter

The near-backscatter by the mutually resonant IAW can deplete both the primary and secondary interaction beams, particularly in intense speckles. This local pump depletion depends jointly on the local intensity of the primary and secondary interaction beams, and reduces the pump intensity available to drive direct backscatter of the primary beam. The calculation of the reduction in the direct SBS backscatter of the primary beam due to the pump depletion from the mutually resonant SBS proceeds as follows. The intensity available in the primary interaction beam for direct backscatter is reduced by the pump, i.e., the dependence of the gain exponent for SBS reflectivity R_{SBS} in Eq.(31) on the input intensity of the primary interaction beam I_1 is replaced by $I_1(1-R_{SBS,12})$ where $R_{SBS,12}=R_1$ is determined by Eq.(34) for SBS. Note that R_{SBS} is a function of I_1 while $R_{SBS,12}$ depends on I_1+I_2. We fit the relation of the pump depletion factor R_1 to the gain exponent (Fig. 10) with a simple rational function to facilitate the numerical average of R_{SBS} with respect to I_1 and I_2 including the pump depletion factor $(1-R_{SBS,12})$. The double integral with respect to I_1 and I_2 is weighted by the speckle intensity PDF (for RPP or filamented beams). For the reference LULI parameters, the direct SBS backscatter reflectivity is significantly reduced (up to ~50% over the range of intensities $<I_2>$) by the local pump depletion due to the mutually resonant two-beam SBS. Plotted in Fig. 13 are the direct backscatter reflectivities as a function of the average intensity of the secondary beam, averaged over normal and filamented speckle distributions for both primary and secondary beams with the average intensity of the primary beam $<I_1>=10^{14}$ W/cm^2 and L_v=300 μm. The magnitude of the reduction in the SBS backscatter in the primary beam with increasing intensity of the secondary interaction beam is similar to that observed in the LULI experiments.

For $<I_2>\rightarrow 0$ the model of gain reduction in SBS backscatter due to the mutually resonant two-beam SBS presented here breaks down because $R_{SBS,12}$ is still quite finite due to its dependence on the primary beam intensity. In the limit of no secondary beam, the near backscatter of the primary interaction beam in the same direction as that due to the mutually resonant ion wave no longer

dominates over direct backscatter; and the near backscatter becomes part of the angular spectrum of the total SBS backscatter of the primary beam which must take into account the angular dependence of the SBS coupling coefficients, the plasma velocity and electron density gradients, and the orientation and dimensions of the speckles. For finite $<I_2>$, the mutually resonant near-backscatter can dominate the direct SBS backscatter; and the pump depletion due to mutually resonant SBS can be significant, which reduces the intensity of the primary interaction beam available for SBS direct backscatter.

If SRS occurs farther into the plasma and closer to the plasma density maximum, it can be inhibited by SBS pump depletion in the intense speckle(s) (length ~ 300 μm) of a single beam or two-beam mutually resonant SBS. Although the overall pump depletion is relatively low due to SBS, the local SBS-induced pump depletion in an intense speckle that would be most susceptible to SRS can be influential in reducing the intensity available to drive the SRS. Consider the local pump depletion of the first laser beam in the presence of a weaker second beam via SBS direct backscatter from the single beam or near-backscatter from the mutually resonant two-beam SBS. The intensity available for SRS is then $\sim(1-R_{SBS})I_{01}^{in}$, where R_{SBS} is the local SBS reflectivity in the speckle. Assuming that SRS wants to occur in the same intense speckle but farther into the plasma, we compute the SRS reflectivity R_{SRS} averaged over the first beam for a given second beam speckle intensity, $<R_{SRS}>_1$ vs. I_2 in Fig. 14a, and R_{SRS} averaged over both beams for a given second beam average intensity $<I_2>$, $<R_{SRS}>_{1,2}$ vs. $<I_2>$ in Fig. 14b. $<I_1>=10^{14}$W/cm^2 in both Fig. 14a and 14b. For this numerical illustration, we have used $R_{SRS}=R$ given in Eq.(34), $\rho=10^{-10}$ and $L_{ne}=5000$ μm in the SRS expressions for the gain exponent following Eq.(34). This is intended to model the weaker linear gradient region nearer the electron density maximum where the SRS emissions are strongest, and the parameters chosen give reasonable values for the SRS backscatter observed in the LULI experiments relevant to this study. There is a significant reduction in the SRS backscatter of the first beam due to SBS pump depletion, and the reduction steadily increases with increasing SBS and increasing intensity of the second beam for LULI parameters.

V. EFFECTS OF SECONDARY NONLINEAR COUPLING ON SBS AND SRS: ION WAVE COUPLING AND LDI

In this section, we address the effects of ion wave mode coupling of SBS decay products on SBS and on SRS when LDI is an important SRS saturation mechanism. The calculations provide quantitative insight into the importance of ion wave mode coupling in the competition of SRS and SBS, and in the multiple laser beam suppression of SBS backscatter of the primary beam.

A. SBS Suppression Due to Ion Wave Mode Coupling

We have numerically integrated the SBS coupled mode equations introduced in Sec. II for two incident laser beams at 1 micron wavelength with the second beam at 22.5˚ with respect to the one dimension of variation (coincident with the propagation direction of the primary laser beam) with SRS suppressed. The LULI observations indicated that the SBS backscatter of the primary laser beam is reduced as a function of increasing laser intensity of the second laser beam. In these numerical integrations we have included IAW mode coupling of all of the decay-product ion waves of the primary and secondary beam SBS interactions (but omitted both pump depletion and shared SBS resonance along the bisector of the two laser beam backscatter directions). The results of a series of calculations are shown in Fig. 15 and indicate a sharp intensity threshold for SBS direct backscatter reduction of the primary interaction beam ($I_2 > 4\times10^{14}$W/cm^2 for $L_{\Delta V}$=300 μm and $I_1=5\times10^{14}$W/cm^2) when the mutually resonant IAW is excluded from the IAW mode coupling. In Fig. 15 we also show the results of a series of calculations including IAW mode coupling between the three IAWs associated with direct backscatter of the primary and secondary interaction beams and their mutually resonant IAW (propagating along the bisector of the two lasers). Here again $I_1=5\times10^{14}$W/cm^2 and I_2 was varied from one computation to the next. The presence of the mutually resonant IAW enhances the effective IAW damping due to mode coupling which significantly increases the SBS suppression effect for direct backscatter of the primary.

The ion wave mode coupling suppression effect relies on the overlap of relatively intense speckles from the two interaction beams. Our quasi-one-dimensional model is valid if the resonance zone lengths h affecting SBS and IAW mode coupling in the interacting speckles are

less than the distance over which the crossing speckles separate by a distance equal to their widths:

$$h \sim (\gamma_s/\omega_s, |\Delta\omega|/\omega_s)_> L_v \sim 30\,\mu m \le 2f\lambda_1/\sin 22.5^\circ \sim 31\mu m, \qquad (38)$$

which is marginally satisfied for the LULI parameters (f=6 and λ_1=1μm). Moreover, the enhanced damping produced is only effective where the SBS interactions have produced decay products of significant amplitude, which begins near the center of the SBS resonance zone and extends in the backscatter direction over the rest of the resonance zone (based on the results of our numerical integrations of the coupled mode equations). We can account for the spatial nonuniformity of the laser intensities due to the speckle intensities in determining the overall SBS suppresion due to ion wave mode coupling in the following model. From the numerical solutions of the SBS+IAW mode coupling equations including the mutually resonant and two backscatter driven IAWs, for $I_1+I_2 \ge 4.5I_0$, $I_0=10^{14}$W/cm^2, there is a gain reduction of up to 1/2 modeled by:

$$G = G_0\{1+0.5[\exp(-\tfrac{I_1+I_2-4.5I_0}{2.5I_0})-1]\} \quad \text{for } I_1+I_2 \ge 4.5I_0 \qquad (39)$$

and $G=G_0=2(I_1/10^{14}\text{W/cm}^2)(L_V/100\mu\text{m})$ for $I_1+I_2<4.5I_0$. The gain reduction leads to a reduction of the backscatter reflectivity which is computed by replacing G_0 in Eq.(34) with the specification of G as a function of I_1+I_2 given here. We then average the resulting reflectivity over the intensity distributions for I_1 and I_2 to obtain beam-averaged SBS reflectivities incorporating the IAW mode-coupling suppression effect.

The results for the SBS direct backscatter reflectivity of the primary interaction averaged over the intensity distribution (either filamented or normal RPP) of the primary interaction beam as a function of the speckle intensity of the second beam is given in Fig. 16a and averaged over the intensity distributions of both beams in Fig. 16b. This incorporates the ion wave mode coupling of the ion wave decay products from the two direct backscatter events and the mutually resonant ion wave. Two overlapping intense speckles from the two interaction beams can reduce the gain significantly, but averaging over the speckle intensity distributions reduces the net effect of the mode-coupling gain reduction. On averaging over the two beams, the SBS reduction as a function of the second beam's average intensity is not as strong as is seen in the experimental observations (compare Figs. 4a and 16b).

B. SRS Model With LDI and Ion Wave Mode Coupling

In LULI exploding foils, SRS should occur preferentially in hot speckles ($I \geq 4I_0$) near the center of the plasma at higher plasma densities and weakest density gradients. For sufficiently high gains and reflectivities, the SRS EPW can satisfy the local threshold conditions for LDI, which then can significantly reduce SRS backscatter. LDI has been observed experimentally in the LULI experiments. The results of numerical integrations of Eqs.(1) and (2) describing SRS and LDI are summarized in Fig. 17 for nominal LULI paramenters for a single laser beam with and without LDI in a linear density gradient. LDI has a very pronounced effect in saturating SRS backscatter when above threshold.

When LDI is active in saturating SRS, our model exhibits an anti-correlation of spatially separated SBS and SRS with respect to the relative strength of the ion wave damping. Increased ion damping reduces SBS and LDI, allowing SRS to increase over a fixed speckle length; and this is illustrated in Eqs.(7), (9-11) in Sec. IIIA. The theoretical justification for these notions are well established and have been argued in the interpretation of experiments.[8,9,21,24,31,34,47] Figure 18 summarizes a series of integrations of the couple mode equations for spatially separated SBS and SRS+LDI for LULI parameters: n_e/n_c=0.1, T_e/T_i~2.4, T_e=0.5 keV, L_{ne} =4000 μm near the plasma center, L_V=280μm, speckle length ~300μm, $<Z>$=3.5, laser intensity for SBS I_{SBS}=4.5x10^{14} W/cm^2, laser intensity for SRS I_{SRS}=4x10^{14}W/cm^2, and with EPW damping rate $\gamma_{EPW}/\omega_{pe}=\nu_{ei}/2\omega_{pe}$~0.001. No pump depletion was allowed in these calculations.

Thomson scattering in the LULI experiments sometimes indicates strong overlap of SBS and SRS backscatter in space-time (e.g., Fig. 5). If LDI is affecting SRS, then IAW mode coupling between SBS and LDI ion waves can contribute to an anti-correlation of SBS and SRS. If SRS and SBS both occur in the same hot speckle, e.g., $I > 4I_0$, the SBS IAW can couple to the LDI IAWs non-resonantly and enhance the IAW damping in both SBS and LDI as illustrated in Eqs.(9-12) leading to reduction of both and an increase in SRS. In Fig. 19 we present results from integrations of the coupled mode equations Eqs.(1-4) for SBS and SRS+LDI with (SBS resonance at 240μm and SRS resonance at 180μm) and without (SBS resonance at 180μm and SRS

resonance at 200μm) efficient cross-coupling of the ion waves from the SBS and LDI interactions. For these calculations, I_{SBS}=5x10^{14} W/cm^2, I_{SRS}=4x10^{14}W/cm^2 and other parameters were the same as those used for the results in Fig. 18 defined in the preceding. There was only a single intense interaction beam driving SBS.

In Fig. 20 we summarize the results of three integrations of the coupled mode equations similar to the coupled SBS and SRS+LDI case shown in Fig. 19 as a function of increasing laser intensity driving SBS. SRS increases significantly for a modest increase in the laser intensity driving SBS because of the damping enhancement in LDI due to the IAW mode coupling produced by the SBS. The parameters are the same as for the results in Fig. 19 except that the SBS intensity has been varied, I_{SBS}~ 5-6×10^{14} W/cm^2.

In the next example (Fig. 21), we include primary and secondary SBS interaction beams overlapping the SRS interaction of the primary interaction beam, but we omit the generation of the mutually resonant IAW. Numerical integrations of the steady-state SBS and SRS mode coupling equations for SBS backscatter by two laser interaction beams (modeling the 22.5˚ relative angle) demonstrated mutual reduction of SBS due to IAW mode coupling and increased SRS (because of increased IAW damping in LDI). IAW mode coupling in the two beams (I_1=5I_0 and I_2=4.6I_0) reduced the backscatter reflectivity of the primary beam from R_{SBS} ~ 1 for single beam to $R_{1,SBS}$=0.39 for the two laser beams present, and IAW mode coupling to LDI increased the SRS reflectivity to 2.5% from 2.1% absent the IAW coupling. The SBS resonance was at 240μm, and the SRS was resonance at 180μm. Although pump depletion is not included in these coupled-mode integrations, it is important to note that with the significant reduction in SBS reflectivities occurring due to enhanced ion wave damping coming from two-beam driven ion wave coupling, more beam intensity is available for SRS farther into the plasma.

We did a series of coupled-mode integrations for the strongly overlapped and coupled SBS and SRS+LDI interactions with two interaction beams in which we varied the intensity of the second interaction beam. The primary interaction beam intensity was held fixed at I_1=4.7I_0, and both SBS and SRS resonance points were at 160 μm. We included the IAW mode coupling by the two

IAWs from the direct backscatter of the two incident beams, the mutually resonant IAW whose propagation bisects the the two laser beams, and the LDI IAW (excited where the SRS was strong enough locally to induce LDI). The ion wave mode coupling led to partial suppression of the primary beam's SBS direct backscatter and enhancement of SRS due to the nonlinearly increased IAW damping helping to inhibit LDI, which increased with increasing I_2 for two overlapping intense speckles. Figure 22 shows the decrease of the SBS backscatter reflectivity and the associated IAW amplitude with increasing I_2, while the SRS reflectivity, the SRS EPW, LDI EPW and IAW amplitudes (driven harder by the SRS EPW), and the mutually resonant SBS IAW amplitudes increase. Thus, the second interaction beam enhances the anti-correlation of SBS and SRS via the ion wave mode coupling mechanism with the provisos that intense speckles from the two interaction beams must be well overlapped and that the SRS and SBS are also well overlapped.

At this point we propose a model that illustrates the leverage that LDI has on the saturation of SRS taking into account the intensity distributions for the speckles in the laser beam. Consider first the saturation of SRS backscatter due to the pump depletion it causes. From Eq.(34) with $G_0 = 1.4I(10^{14}W/cm^2)L_{ne}(1000\mu m)$ for SRS, we determine the reflected power as a function of the laser beam intensity through the gain parameter. For this example we used L_{ne}=5000 μm to obtain plausible values of the SRS reflectivity for the LULI experiments. Our single-speckle coupled-mode integrations including saturation of SRS by LDI suggest the following model of SRS gain reduction: $G_{SRS}=G_0(I)[1+\alpha(I-I_{LDI})/I_c]^{-1}$, where $\alpha=0$ for $I<I_{LDI}$ and $\alpha=1$ for $I\geq I_{LDI}$ above the LDI threshold, and I_c is determined by fitting to the set of numerical integrations of our coupled mode equations for SBS, SRS and LDI. We substitute this G_{SRS} into Eq.(34) and numerically invert for the relation of the SRS reflectivity as a function of the reduced gain and, hence, the laser intensity I. We then compute the average of R_{SRS} with respect to beam intensity I for RPP and filamented speckle distributions with $\langle I\rangle=I_0=10^{14}$W/cm^2, $I_{LDI}=2I_0$ or ∞ (no LDI), and different values of I_c. Figure 23 shows the results of the beam-averaged SRS reflectivities for filamented and RPP beams as a function of the input laser intensity $\langle I\rangle=\langle I_{in}\rangle$ with and without LDI and a larger value of $I_c=3I_0$ to model the inhibition of LDI by two laser-beam driven ion-wave

mode coupling or turbulent detuning that weakens the reduction of the SRS gain. This model calculation demonstrates that LDI can have a profound effect in saturating SRS backscatter, and LDI inhibition can significantly increase SRS reflectivity over its saturated value when LDI is not inhibited.

VI. ENERGY TRANSFER BY NEAR-FORWARD STIMULATED BRILLOUIN SCATTERING

We have calculated the possibility of the two-laser-beam resonant nonlinear excitation (optical mixing) of an IAW in the presence of flow and the concomitant energy transfer from one beam to the other. If there is a resonance that is not detuned, there can be finite energy transfer between the two beams which has a strong dependence on both laser-beam intensities. If a second weaker interaction beam can transfer significant amounts of energy from a stronger primary beam, this can reduce the primary beam's ability to undergo direct SBS backscatter. This physics is of considerable interest in applications of multiple crossing laser beams for indirect drive laser fusion experiments where significant energy transfer between the crossing beams will disturb the uniform distribution of laser energy deposition required for efficient capsule implosions.

When the beat wave of two overlapping laser beams of equal frequency in the presence of flows satisfy resonance with an acoustic wave, energy transfer can result.[24-28] The resonance condition is $\omega_1-\omega_2=0=\pm|\mathbf{k_1}-\mathbf{k_2}|c_S+(\mathbf{k_1}-\mathbf{k_2})\cdot\mathbf{v_{drift}}$. For the primary and secondary interaction beams in the LULI experiments, the scattering geometry is pictured in Fig. 24. Because the primary flow is normal to the exploding foil near the foil, which is anti-parallel to the primary interaction beam, the sound wave makes an oblique angle with the flow and satisfies resonance in a layer where $v_{drift}\sim 2.5c_s$ ($c_s\sim 1.7\times10^7$cm/s at 2 ns), which in Fig. 7 is at some distance from the foil (500-800μm) when the interaction beams are at their peak intensities. A one-dimensional model of the flow and the resonant interaction may not be entirely reliable, and multi-dimensional physics effects may be significant. Nevertheless, we will proceed with a calculation of the interaction based on the one-dimensional model of the expanding plasma. Rose and Ghosal[48] have calculated aspects of the beam energy transfer of two crossing RPP beams in a flowing plasma using a very different

mathematical approach for the RPP physics. Their calculation uses a statistical ensemble of RPP beamlets and a paraxial approximation, and neglects spatial gradients in the plasma and the flow. Rose and Ghosal obtain an energy transfer expression for particular plasma parameters, finite ion acoustic damping, and for equal beam intensities in well separated beams. They also obtain results for intra-beam interactions with the flow leading to beam bending. Our calculation omits beam bending, but assumes that the flow near resonance has a linear gradient which is appropriate for the LULI exploding foil experiments. In our model RPP physics is captured qualitatively with a probability distribution function for the speckle intensity.

The action transfer (gain) parameter for the energy transfer can be readily calculated from Eq.(33) for a one-dimensional (parallel to the primary interaction beam) steady-state model:

$$G = (\pi^2/4k_s^2\lambda_e^2)(k_s/k_1)^2(L_v/\lambda_1)(v_{01}/c)^2 \rightarrow G \sim O(1/2)\,L_v/100\mu m \qquad (40)$$

For incident laser powers $I_2 << I_1$, G is just the Rosenbluth linear gain exponent for growth in wave power of the second beam due to forward scattering by the primary beam. A reasonable estimate for the velocity scale length at 2 nsec is L_v=300μm (Fig. 7). Appreciable energy transfer (20-30% depending on I_2^{in}/I_1^{in}) can occur if there is a resonance and if it is not detuned. Detuning of the acoustic resonance is significant when $|\Delta\omega| \geq \gamma_s \sim 0.1\omega_s$. Thus, 10% fluctuations in v_{drift} or c_s would detune the resonance appreciably. Electron density fluctuations lead to $\Delta\omega \sim \Delta k_{1,2}c \sim (1/2)\omega_{1,2}\,(n_e/n_{crit})|\delta n/n_e|$ The LULI experimental measurements of "thermal" fluctuations give $\delta n_{rms}/n_e \sim 0.3\times10^{-3}$, which leads to $\Delta k_{1,2}c \sim 0.6\times10^{-11}s^{-1} > \gamma_s \sim 0.4\times10^{-11}s^{-1}$. This reduces the effective energy transfer gain parameter to $G_{eff}=G/(1+\Delta\omega^2/\gamma_s^2)\sim 0.3G\sim$O(1/2), and 10% energy transfer can occur for $I_2^{in}/I_1^{in}\sim 0.1$ in this circumstance. We note that the two interaction beams can still undergo mutually resonant SBS near-backscatter with a different mix of intensities in the two interaction beams due to the optical mixing than was incident on the edge of the plasma.

So far the calculation of crossed-beam energy transfer has tacitly assumed that the two beams have uniform intensities equal to their average intensities. A more realistic model of the relative energy transfer takes into account the nonuniformity of the laser beams. We average the energy

transfer's dependence on the input laser intensities over the speckle intensity probability distributions of the two beams. We use the RPP and filamented intensity distributions introduced in Sec. IIIB shown in Fig. 11. If there is no resonance detuning, then the relative energy transfer from the primary interaction beam to the second interaction beam is determined implicitly by R in the following expression[48] for forward scattering energy transfer for nominal LULI parameters:

$$G = (1+\rho)^{-1}\ell n[(\rho + R)/(\rho - \rho R)], \qquad (41)$$

where $G \sim 1.5(I_1^{in}/10^{14} W/cm^2)(L_v/300\,\mu m)$, $R = \Delta I_1 / I_1^{in}$, and $\rho = I_2^{in} / I_1^{in}$. The applicability of Eqs.(40) and (41) depend on whether the resonance zone width for the near-forward SBS interaction is less than the distance in which the crossing beam speckles separate by more than their widths, which gives the same condition as is set forth in Eq.(38) and is marginally satisfied. The dependence of Eq.(41) on intensity and power input ratio ρ is dictated by wave action conservation,[49] and the beam energy transfer expressions calculated by Rose and Ghosal[48] are consistent with this. We next numerically fit a simple function to $R(I_1^{in}, I_2^{in})$ and compute the average of R with respect to I_1^{in} and I_2^{in}. Solutions for R vs. G from Eq.(41) and the beam-averaged values of $<R>$ vs. $<I_2^{in}>$ for $<I_1^{in}>=10^{14}$ W/cm^2 are shown in Fig. 25 for both filamented and RPP intensity distributions. The filamented intensity distributions lead to slightly less energy transfers because the effective value of the input ratio ρ is reduced. The predicted energy transfers exceed 20% of the primary interaction beam for $I_2^{in}/I_1^{in}>10\%$, and there could be as much as ~55% energy transfer for $I_2^{in}/I_1^{in}=0.8$. Because we have assumed that there is a strong resonance with no detuning, these values of energy transfer likely over-estimate the energy transfer to be realized in the experiments. LULI observations reported in Ref. 7 indicate significant enhancement of the light scattered in the forward direction parallel to the second interaction beam. Reference 7 also includes a discussion and an analysis of the spectral features of the forward scattered light.

If we reduce the SBS backscatter gain parameter for the primary beam by the depletion accomplished by the optical mixing, $G_{SBS} \rightarrow G_{SBS}[1 - R(I_1^{in}, I_2^{in})]$, and for the optical mixing gain parameter G in Eq.(40) use $G \sim 0.5(I_1^{in}/10^{14} W/cm^2)(L_v/300\,\mu m)$ that has been detuned by the thermal density fluctuations as estimated in the preceding, we can compute the SBS direct

backscatter of the primary beam as reduced by optical mixing averaged over the speckle intensity distributions (RPP or filamented) of both primary and secondary interaction beams. This is plotted in Fig. 25c. These results suggest that the optical mixing can have a very strong suppression effect on the primary beam's SBS direct backscatter for LULI conditions if the optical mixing resonance occurs. The strength of the suppression effect is comparable to that observed in the experiment (compare Figs. 3 and 25c).

VII. CONCLUSIONS

In this paper, analytical and numerical solutions of the coupled mode equations describing SRS, SBS, LDI, and IAW coupling have been presented for the purpose of modeling experiments in the LULI laser-plasma facility. The focus of the paper has been to elucidate a few nonlinear mechanisms that can influence the competition of SBS and SRS in multiple beam experiments. The principal conclusions are as follows.

SBS and SRS convective gains can be appreciable (≥5) in intense speckles in LULI laser beams ($I \geq 4\text{-}5 I_0$) illuminating CH foils. Because EPW linear damping is weak, LDI thresholds are low and LDI influences SRS saturation for small LDI IAW amplitudes: $|\delta n_{esLD}/n_{0e}| \geq 0.004$. Thermal and ponderomotive self-focusing should significantly increase the laser intensity in the speckles and deform the local electron density (a possibly important detuning mechanism for SRS[31] that has been omitted in our model). Spatial inhomogeneities in the flow and electron density limit SBS and SRS backscatter, respectively. Generally, SBS and SRS are anti-correlated in time in the experiments, sometimes well separated spatially and sometimes overlapping. SBS occurs preferentially nearer the plasma edge and SRS preferentially near the plasma center where the electron density peaks. The SRS-active region is relatively narrow at first and widens as the plasma expands away from the foil, and SBS always occurs first. If the SBS and SRS regions overlap, the scattering of the SRS EPW by the SBS IAW into a damped EPW is an additional damping mechanism for the SRS EPW (similar to the additional damping afforded by the LDI). Although this coupling appears to be reasonably strong for LULI parameters (if the overlap condition is met),

its influence on SRS is weaker than the LDI saturation mechanism by a factor of ~5 in the IAW wave amplitude for the nominal LULI parameters.

IAW mode coupling driven by the IAW decay products in overlapping high-intensity speckles in multiple beams enhances IAW damping in SBS and LDI, which in turn reduces the SBS gain exponent and increases the SRS gain exponent. There can be significant IAW damping enhancements for localized peak IAW amplitudes $|\delta n_{es}/n_{0e}|\sim 0.2$. The inclusion of the mutually resonant SBS IAW of two interaction beams enhances the effects of ion wave mode coupling. LDI helps saturate SRS at lower levels for LULI parameters. If SBS and SRS overlap, then IAW mode coupling between the SBS and LDI IAWs can lead to an additional dissipation for these IAWs which limits both SBS and LDI. By limiting LDI to lower amplitudes, IAW mode coupling leads to a weakening of the SRS saturation mechanism; and SRS can grow to higher amplitudes. Thus, IAW mode coupling provides an SRS+SBS anti-correlation mechanism. However, because this mechanism depends on the overlap of intense speckles, we must take into account the beam intensity probability distributions and average the mode coupling effects over these distributions to get a more realistic quantitative assessment. Our mode coupling model determines that with increasing average beam intensity of the secondary interaction beam, the SBS reflectivity decreases by up to ~25% for $<I_2>$ approaching $0.8I_0$, which is not as strong as the 50% reduction seen in the experiment. It would be desirable to obtain space-time resolved measurements of the correlation and anti-correlation of the principal transverse and longitudinal waves and their beat waves in the experiments to compare to the predictions of the IAW mode coupling model.

The intense speckles that are SBS and/or SRS active can be intense enough for finite local pump depletion. Local SBS pump depletion from near-backscatter SBS by the mutually resonant IAW can be significant (>10% for $I_1+I_2>4\times10^{14}$W/cm^2) and increases with the power of the second beam. However, averaging over both I_1 and I_2 leads to only 1-3% pump depletion overall (depending on the speckle intensity distribution). Nevertheless, local SBS pump depletion in a hot speckle nearer the plasma edge due to the mutually resonant IAW can limit direct SBS backscatter of the primary interaction beam and SRS backscatter occurring farther into the plasma. With

averaging over model speckle intensity distributions, there is a ~30% reduction in the primary SBS backscatter for $<I_2>=0.4I_0$ and a ~50% reduction for $<I_2>=0.8I_0$. There is a ~30% reduction in SRS backscatter reflectivity for $<I_2>=0.25I_0$ due to pump depletion by the mutually resonant SBS interaction. This is a credible SBS/SRS anti-correlation mechanism for the LULI experimental conditions. Moreover, when multiple-beam SBS suppression limits SBS pump depletion, then more energy reaches the SRS-active region closer to the plasma center allowing increased SRS in our model. Indeed, the SRS signal is enhanced in LULI observations with multiple beams when SBS suppression is observed.

Optical mixing of the two laser beams may be able to satisfy resonance conditions with the flowing plasma 500-800μm from the foil location, which can contribute to suppressing SBS backscatter in the primary interaction beam. The energy transfer increases with the intensities of the beams and is very sensitive to detuning and to the directionality of the flow essential for resonance. The beam intensities in the LULI experiments are sufficient that appreciable energy transfers (10-20% of the primary beam or more) can be realized if there is a resonance that is not detuned. For $<I_2>=0.8I_0$ as much as ~55% of the primary beam energy might be transferred to the secondary beam. Moreover, we have calculated the pump depletion effect of the optical mixing on the SBS direct backscatter, which indicates that there can be significant suppression of the SBS with a strong dependence on the average intensity of the second interaction beam. In Ref. 7 significant enhancement of the transmitted forward scattered light in the direction of the second interaction beams when two interaction beams were present has been reported and some analysis and interpretation of the spectra is given.

ACKNOWLEDGMENTS

We are grateful to A. Bruce Langdon and other members of the scientific staff at the Lawrence Livermore National Laboratory, and to V. Tikhonchuk and C. McKinstrie for useful discussions, insight, and encouragement in this work. We also thank the technical and scientific groups at LULI for their support. We thank the referee for many valuable comments.

This work was performed for the U.S. Department of Energy under Contract No. W-7405-ENG-48 partially through the Institute for Laser Science and Applications at the University of California Lawrence Livermore National Laboratory.

References

[1]C. Labaune, H. A. Baldis, N. Renard, E. Schifano, A. Michard, Phys. Rev. Letters, **76**, 3727 (1996).

[2]N. Renard, C. Labaune, H. A. Baldis, B. S. Bauer, B.Quesnel, E. Schifano, A. Michard, W. Seka, and K.G. Estabrook, Phys. Rev. Lett. **77**, 3807 (1996).

[3]C. Labaune, H. A. Baldis, N. Renard, E. Schifano, A. Michard, Phys. Rev. Letters, **76**, 3727 (1996).

[4]C. Labaune, H. A. Baldis, N. Renard, E. Schifano, A. Michard, Phys of Plasmas, **4**, 423 (1997).

[5]C. Labaune, H. A. Baldis, B. Bauer, V. T. Tikhonchuk, G. Laval, Phys of Plasmas, **5**, 234 (1998).

[6]H. A. Baldis, C. Labaune, E. Schifano, N. Renard, and A. Michard, Phys. Rev. Lett. **77**, 2957 (1996).

[7]C. Labaune, H. A. Baldis, B. I. Cohen, W. Rozmus, S. Depierreux, E. Schifano, B. S. Bauer, and A. Michard, Plasmas **6**, 2048 (1999); C. Labaune, H. A. Baldis, B. S. Bauer, E.Schifano, and B. I. Cohen, Phys. Rev. Lett. **82**, 3613 (1999).

[8]H. A. Baldis, D. M. Villeneuve, B. La Fontaine, G. D. Enright, C. Labaune, S. Baton, Ph. Mounaix, D. Pesme, M. Casanova, and W. Rozmus, Phys. Fluids B **5**, 3319 (1993); R. K. Kirkwood, B.J. MacGowan, D. S. Montgomery, *et al*., Phys. Rev. Lett. **77**, 2706 (1996); D. S. Montgomery, B. B. Afeyan, J. A. Cobble, *et al*., Phys. of Plasmas **5**, 1973 (1998)

[9]R. L. Berger, C. H. Still, E. A. Williams, and A. B. Langdon, Phys. Plasmas **5**, 4337 (1998); R.L. Berger, E. Lefebvre, A.B. Langdon, J.E. Rothenberg, C.H. Still, and E.A. Williams, Phys. Plasmas **6**, 1043 (1999).

[10]J. F. Drake, P. K. Kaw, Y. C. Lee, G. Schmidt, C. S. Liu, and M. N. Rosenbluth, Phys. Fluids **17**, 778 (1974); D. W. Forslund, J. M. Kindel, and E. L. Lindman, Phys. Fluids **18**, 1002 (1975).

[11]B. I. Cohen and C. E. Max, Phys. Fluids **22**, 1115(1979).

[12]W. L. Kruer, *The Physics of Laser Plasma Interactions* (Addison-Wesley, Reading, Mass., 1988).

[13]B. I. Cohen, B. F. Lasinski, A. B. Langdon, and E. A. Williams, Phys. Plasmas **4**, 956 (1997).

[14]R. L. Berger, B. F. Lasinski, T. B. Kaiser, E. A. Williams, A. B. Langdon, and B. I. Cohen, Phys. Fluids B **5**, 2246 (1993).

[15]J. D. Lindl, Phys. Plasmas **2**, 3933 (1995).37 (1997).

[16]National Tech. Info. Service Document Nos. DE95017671-DE95017673 and DE95017676-DE95017700 (J. A. Paisner, E. M. Campbell, and W. J. Hogan, The Nat. Ignition Facility Project, UCRL-JC-117397 and UCRL-PROP-117093, May, 1994). Copies may be obtained from Nat. Tech. Inf. Service, Springfield, VA 22161;

[17]B. I. Cohen, B. F. Lasinski, A. B. Langdon, E. A. Williams, H. A. Baldis, and C. Labaune, Phys. Plasmas **5**, 3402 (1998).

[18]H. A. Rose, D. F. DuBois, and B. Bezzerides, Phys. Rev. Lett **58**, 2547 (1987).

[19]K. Estabrook, W. L. Kruer, and M. G. Haines, Phys. Fluids B **1**, 1282 (1989).

[20]H. A. Baldis, D. M. Villeneuve, C. Labaune, D. Pesme, W. Rozmus, W. L. Kruer, and P. E. Young, Phys. Fluids B **3**, 2341 (1991).

[21]B. Bezzerides, D. F. DuBois, and H. A. Rose, Phys. Rev. Lett. **70**, 2569 (1993).

[22]H. A. Rose, Phys. Plasmas **4**, 437 (1997).

[23]V. T. Tikhonchuk, C. Labaune, and H. A. Baldis, Phys. Plasmas **3**, 3777 (1996); V. T. Tikhonchuk, Ph. Mounaix, and D. Pesme, Phys. Plasmas **4**, 2658 (1997).

[24]R.K. Kirkwood, B.B. Afeyan, W.L. Kruer, B.J. MacGowan, J.D. Moody, D.S. Montgomery, D.M. Pennington, T.L. Weiland, and S.C. Wilks, Phys. Rev. Lett. **76**, 2065 (1996); W. L. Kruer, S. C. Wilks, B.B. Afeyan, and R.K. Kirkwood, Phys. Plasmas **3**, 382 (1996).

[25]R. K. Kirkwood, B. J. MacGowan, D. S. Montgomery, B. B. Afeyan, W.L.Kruer, D.M.Pennington, S.C. Wilks, J.D. Moody, K. Wharton, C.A. Back, K.G. Estabrook, S.H. Glenzer, M.A. Blain, R.L. Berger, D.E. Hinkel, B.F. Lasinski, E.A .Williams, D. Munro, B.H. Wilde, and C. Rousseaux, Phys. Plasmas **4**, 1800 (1997).

[26]K.B. Wharton, R.K. Kirkwood, S.H. Glenzer, K.G. Estabrook, B.B. Afeyan, B.I. Cohen, J.D. Moody, and C. Joshi, Phys. Rev. Lett. **81**, 2248 (1998); K. B. Wharton, R. K. Kirkwood, S. H.

Glenzer, K. G. Estabrook, B. B. Afeyan, B. I. Cohen, J. D. Moody, B. J. MacGowan, and C. Joshi, Phys. Plasmas **6**, 2144(1999); B.B. Afeyan, C. Geddes, D. S. Montgomery, R. K. Kirkwood, *et al*., "Optical Mixing Controlled Stimulated Scattering Instabilities: Progress Toward Control of SRS and SBS Scattering Levels with Overlapping Beams in ICF Targets," in *Inertial Fusion Sciences and Applications 99* (Elsevier, Paris, France, 2000), eds. C. Labaune, W. Hogan, and K. Tanaka, p. 331.

[27]B. I. Cohen, B. F. Lasinski, A. B. Langdon, E. A. Williams, K. B. Wharton, R. K. Kirkwood, and K. G. Estabrook, Phys. Plasmas **5**, 3408 (1998).

[28]C. J. McKinstrie, A. V. Kanaev, V. T. Tikhonchuk, R. E. Giacone, and H. X. Vu, Phys. Plasmas **5**, 1142 (1998).

[29]H. H. Klein, E. Ott, and W. M. Manheimer, Phys. Fluids **18**, 1031 (1975); D. W. Forslund, J. M. Kindel, and E. L. Lindman, Phys. Fluids **18**, 1017 (1975); B. I. Cohen and A. N. Kaufman, Phys. Fluids **20**, 1113 (1977); B. I. Cohen and A. N. Kaufman, Phys. Fluids **21**, 404 (1978); K. Y. Sanbonmatsu, H. X. Vu, B. Bezzerides, and D. F. DuBois, Phys. Plasmas **7**, 1723 (2000); K. Y. Sanbonmatsu, H. X. Vu, D. F. DuBois, and B. Besserides, Phys. Plasmas **7**, 2824 (2000).

[30]H. X. Vu, Phys. Plasmas **4**, 1841 (1997); R. E. Giacone and H. X. Vu, Phys. Plasmas **5**, 1455 (1998); C. Riconda, S. Huller, J. Myatt, and D. Pesme, Physics Scripta **T84**, 217 (2000).

[31]T. Kolber, W. Rozmus, and V. T. Tikhonchuk, Phys. Fluids **B5**, 138 (1993); D. A. Russell, D. F. DuBois, and H. A. Rose, Phys. Plasmas **6**, 1294 (1999).

[32]J. A. Heikkinen, S. J. Karttunen, and R. R. E. Salomaa, Phys. Fluids **27**, 707 (1984).

[33]A. V. Maximov, W. Rosmus, V. T. Tikhonchuk, D. F. DuBois, H. A. Rose, and A. M. Rubenchik, Phys. Plasmas **3**,1689 (1996).

[34]R. P. Drake and S. H. Batha, Phys. Fluids **B 3**, 2936(1991).

[35]M. N. Rosenbluth, Phys. Rev. Lett. **29**, 565 (1972).

[36]A. N. Kaufman and B. I. Cohen, Phys. Rev. Lett. **30**, 1306 (1973).

[37]G. B. Zimmerman and W. L. Kruer, Comments Plas. Phys. **2**, 51 (1975).

[38]K. Estabrook, W. L. Kruer, and E. A. Williams, Phys. Fluids **31**, 372 (1988); E. A. Williams and T. W. Johnston, Phys. Fluids B **1**, 188 (1989).

[39]E. A. Williams, J. R. Albritton, and M. N. Rosenbluth, Phys. Fluids **22**, 139 (1979).

[40]T. B. Kaiser, B. I. Cohen, R. L. Berger, B. F. Lasinski, A. B. Langdon, and E. A. Williams, Phys. Plasmas **1**, 1287 (1994); E. M. Epperlein, Phys. Rev. Lett. **65**, 2145 (1990); E. M. Epperlein, R. W. Short, and A. Simon, Phys. Rev. Lett. **69**, 1765 (1992).

[41]M. Curtet and G. Bonnaud, C. R. Acad. Sci., Ser. IIb, **327**, 799 (1999); M. Curtet and G. Bonnaud, Phys. Rev. E **5**, 5052 (1999).

[42]R.L. Berger, E. A. Williams, and A. Simon, Phys. Fluids B **1**, 414 (1989); L. Divol and P. Mounaix, Phys. Plasmas **6**, 4037 (1999).

[43]C. L. Tang, J. Appl. Phys. **37**, 2945 (1966).

[44]J. W. Goodman, *Statistical Optics* (Wiley, New York, 1985).

[45]S. P. Obenschain, C. Pawley, A. Mostovych, J. Stamper, J. H. Gardner, A. J. Schmitt, and S. E. Bodner, Phys. Rev. Lett. **62**, 768 (1989).

[46]V. T. Tikhonchuk, S. Huller, and Ph. Mounaix, Phys. Plasmas **4**, 4369 (1997).

[47]J. C. Fernandez, J. A. Cobble, B. H. Failor, D. F. DuBois, D. S. Montgomery, H. A. Rose, H. X. Vu, B. H. Wilde, R. E. Chrien, Phys. Rev. Lett. **77**, 2702 (1996);

[48]H. A. Rose and S. Ghosal, Phys. Plasmas **5**, 1461 (1998).

[49]B. I. Cohen, Comments Plasma Phys. Controlled Fusion **8**, 197(1984).

Figure Captions

Figure 1. Influence of multiple-beam irradiation on the amplitude of ion acoustic waves associated with stimulated Brillouin scattering in LULI experiments. Reduction of the SBS IAW amplitude with multiple beams.

Figure 2. Influence of mulitple-beam irradiation on the amplitude of electron plasma waves associated with stimulated Raman scattering in LULI experiments. Increase of the SRS EPW amplitude with multiple beams.

Figure 3. SBS of the main interaction beam is reduced by the presence of the second interaction beam in LULI experiments.

Figure 4. Modification of the intensity of the scattered light from the IAW and EPW as a function of the intensity of the secondary laser beam in LULI experiments.

Figure 5. Space-time evolution of Thomson scattered light from SBS ion waves and SRS electron plasma waves modified by crossed beam irradiation in LULI experiments: EPWs associated with SRS start earlier in the laser pulse with multiple beams than with a single interaction beam, and coexist with IAWs associated with SBS.

Figure 6. Schematic of mode coupling of LDI, SRS, and SBS by ion waves.

Figure 7. LASNEX simulation results for a LULI exploding CH foil plasma.

Figure 8. SBS backscatter calculation for a single laser beam in LULI nominal plasma conditions: reflectivity and relative electron density perturbation as a function of laser intensity with no pump depletion. The dashed line indicates the Rosenbluth convective amplification.

Figure 9. SRS backscatter calculation for a single laser beam in LULI nominal plasma conditions: reflectivity and relative electron density perturbation as a function of laser intensity with no pump depletion. The dashed line indicates the Rosenbluth convective amplfication.

Figure 10. The power reflectivity R for backscatter as a function of the total gain parameter G_t including pump depletion.

Figure 11. Model speckle intensity probability distribution functions as a function of local intensity relative to the average intensity I/I_0.

Figure 12. The power reflectivity for two-beam mutually resonant near-backscatter SBS averaged over both interaction beams as a function of the second interaction beam intensity for $\langle I_1 \rangle = 10^{14}$W/cm^2, LULI reference plasma conditions, and either filamented or RPP beams.

Figure 13. Single-beam SBS direct backscatter reflected power averaged over the intensity distribution with $\langle I_1 \rangle = 10^{14}$W/cm^2 and inhibition due to two-beam mutually resonant SBS pump depletion as a function of the second beam average intensity.

Figure 14. Beam averaged SRS backscatter reflected power for a single beam as inhibited by two-beam mutually resonant SBS pump depletion with $\langle I_1 \rangle = 10^{14}$W/cm^2 and either RPP or filamented intensity distributions (a) as a function of speckle intensity of the second beam and (b) averaged over the second beam intensity distribution as a function of $\langle I_2 \rangle$.

Figure 15. Single-beam SBS direct backscatter reflectivity and relative electron density perturbation (rms and peak) local to a speckle for $I_1 = 5\times10^{14}$W/cm^2 and reference LULI conditions as inhibited by ion wave mode coupling with SBS ion waves of a second interaction beam as a function of the second beam local speckle intensity.

Figure 16. (a) Single-beam SBS direct backscatter reflectivity averaged over the primary beam for $\langle I_1 \rangle = 10^{14}$W/cm^2 and reference LULI conditions as inhibited by ion wave mode coupling with SBS ion waves of a second interaction beam as a function of the second beam local speckle intensity. (b) The SBS backscatter reflectivity averaged over both primary and secondary interaction beams for RPP and filamented beams.

Figure 17. Single-beam SRS direct backscatter reflectivity and relative electron density perturbation (rms and peak) local to a speckle with and without LDI saturation as a function of beam intensity for LULI reference plasma conditions.

Figure 18. Single-beam SBS and SRS direct backscatter reflectivities and relative density perturbations in a single speckle as a function of relative IAW damping rate for spatially separated SRS and SBS resonances, and with LDI active as an SRS saturation mechanism. SRS and SBS are anti-correlated with respect to IAW damping.

Figure 19. Single-beam SBS and SRS direct backscatter electromagnetic wave fields and relative electron density amplitudes as functions of position with and without coupling of SBS to SRS/LDI via IAW nonlinear mode coupling from a single-speckle calculation. There is no pump depletion.

Figure 20. Single-beam SRS direct backscatter reflectivities and relative electron density amplitudes (peak and rms) from three single-speckle calculations with coupling of SBS to SRS/LDI via IAW nonlinear mode coupling as a function of SBS beam intensity for a scale length L_v=280μm. There is no pump depletion.

Figure 21. Single-beam SRS/LDI direct backscatter electromagnetic wave fields and relative electron density amplitudes as functions of position with coupling of two-beam SBS to SRS via IAW mode coupling (omitting the mutually resonant IAW) and with I_1=5×10^{14}W/cm^2 and I_2=4.6×10^{14}W/cm^2 and LULI reference plasma conditions.

Figure 22. SBS and SRS primary interaction beam direct backscatter reflectivities and relative electron density perturbations for I_1=4.7×10^{14}W/cm^2 as a function of the second SBS beam intenstiy I_2 from a series of single-speckle calculations including IAW mode coupling from both SBS backscatter IAWs and the mutually resonant IAW. There is no pump depletion.

Figure 23. SRS direct backscatter reflectivity averaged over the beam intensity distribution as a function of the incident average laser intensity without and without LDI, and with partial inhibition of LDI.

Figure 24. Schematic of near-forward stimulated Brillouin scattering and the resonant drift velocity required to couple two equal-frequencies laser beams.

Figure 25. (a) Energy transfer fraction R as a function of the gain parameter G for forward scattering. (b) The beam-averaged relative energy transfer as a function of the second beam average intensity for two RPP beams with $\langle I_1^{in}\rangle$=10^{14}W/cm^2 and LULI reference conditions. (c) Beam-averaged SBS backscatter reflectivity reduced by optical mixing as a function of $\langle I_2^{in}\rangle$ for filamented and RPP beam intensity distributions.

Figure 1

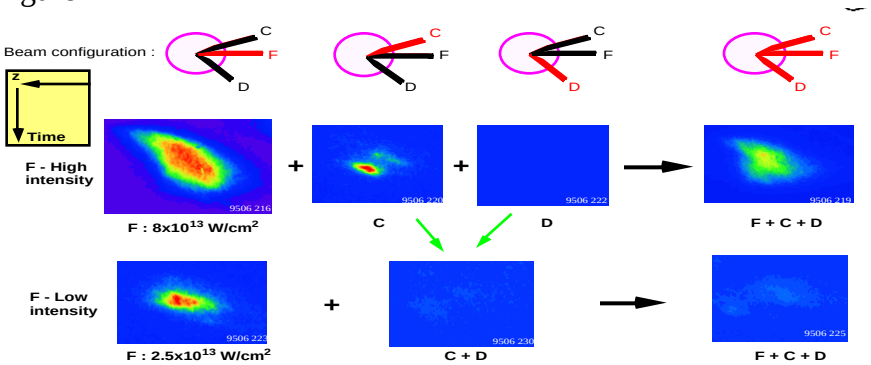

Figure 2

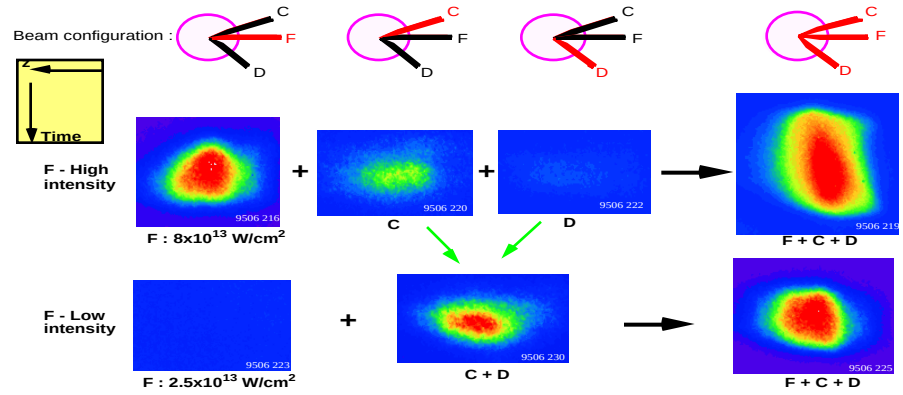

Figure 3

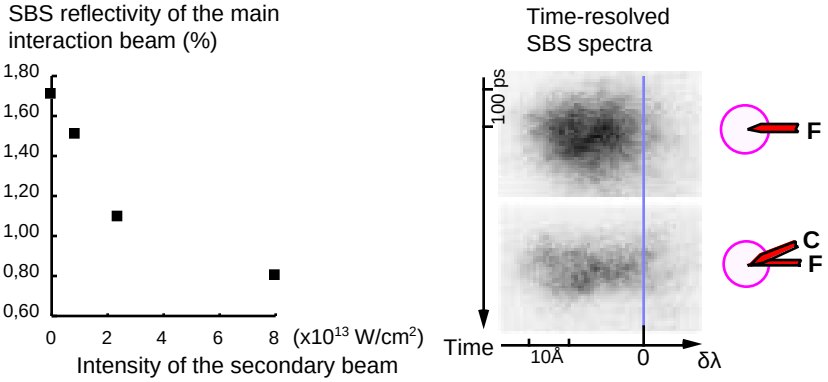

Figure 4

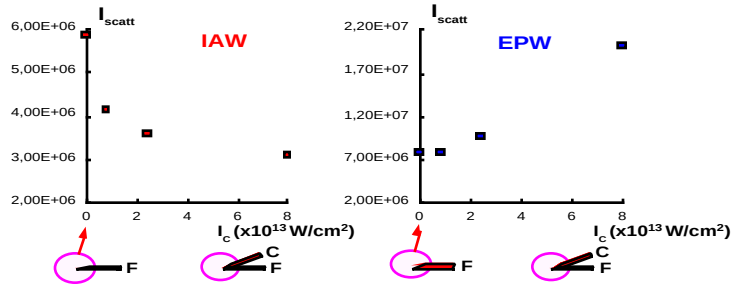

Figure 5

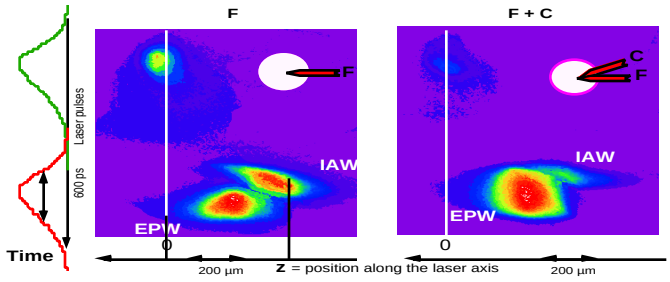

Figure 6

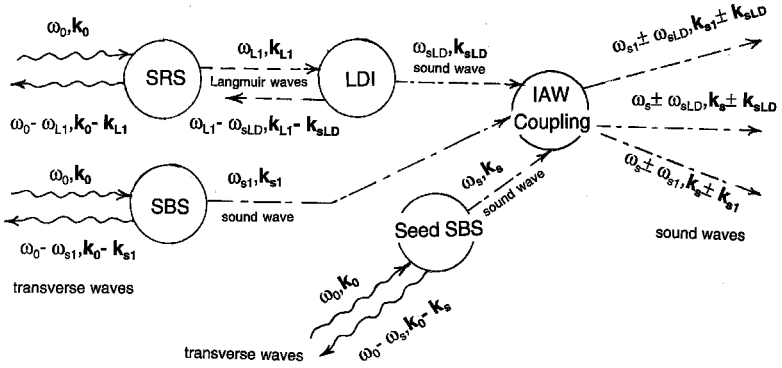

Figure 7

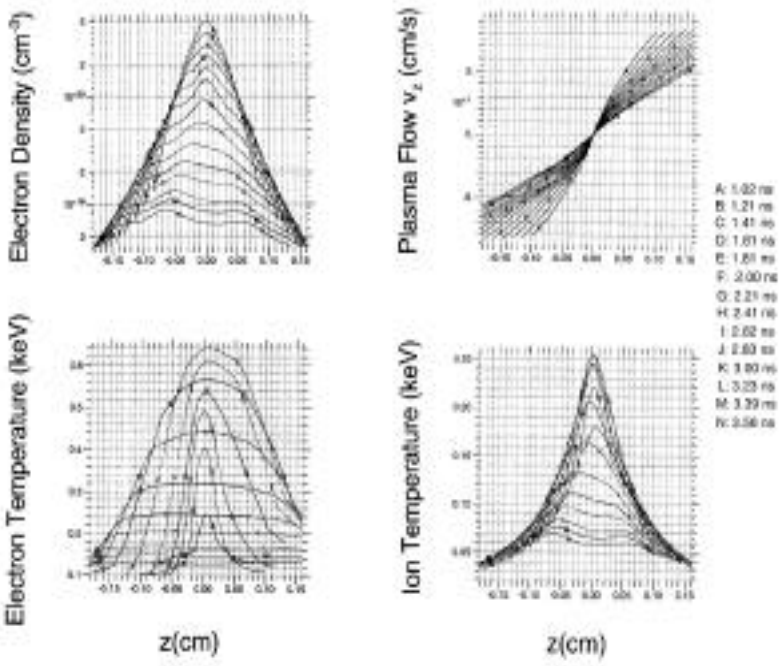

Figure 8

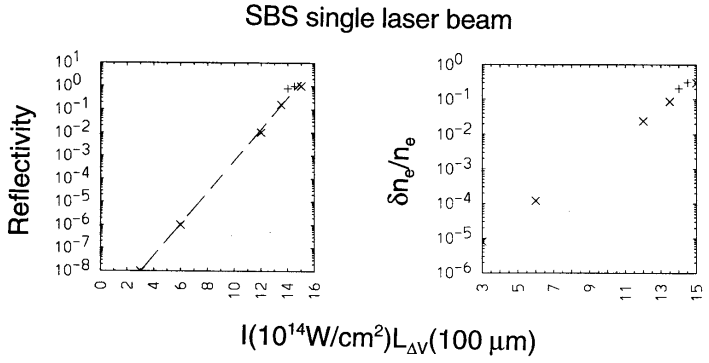

Figure 9

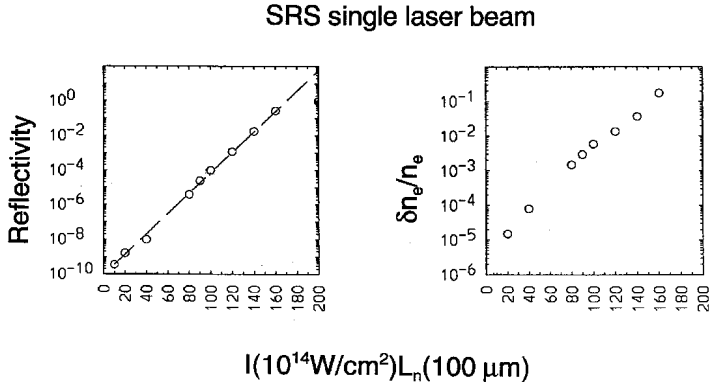

Figure 10

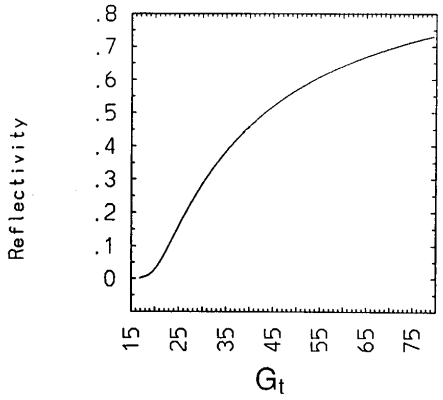

Figure 11

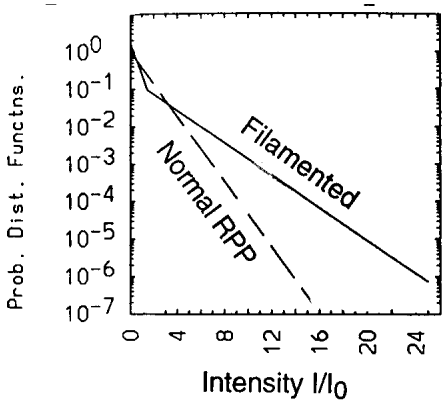

Figure 12

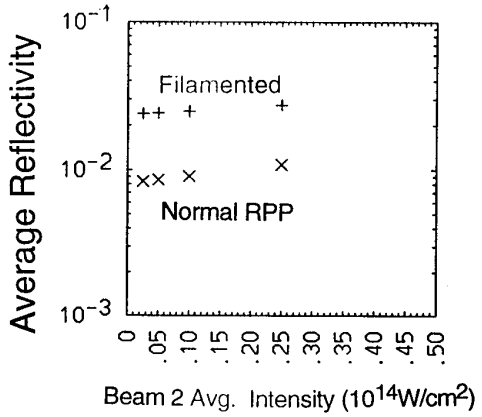

Figure 13

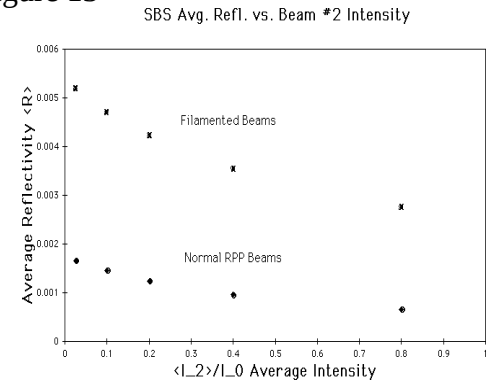

Figure 14

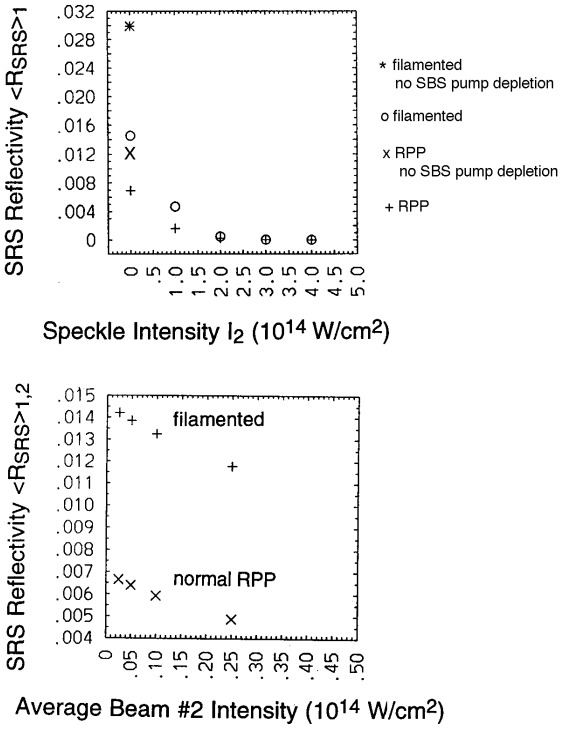

Figure 15

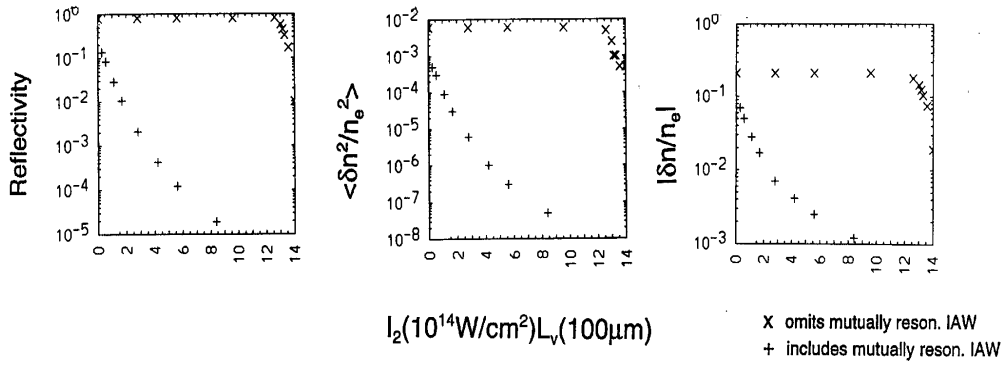

Figure 16

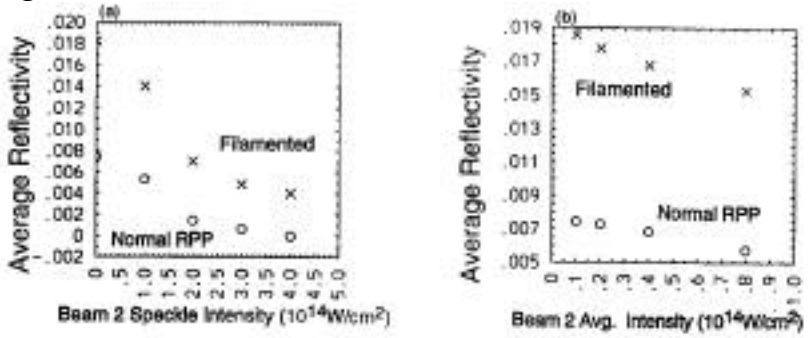

Figure 17

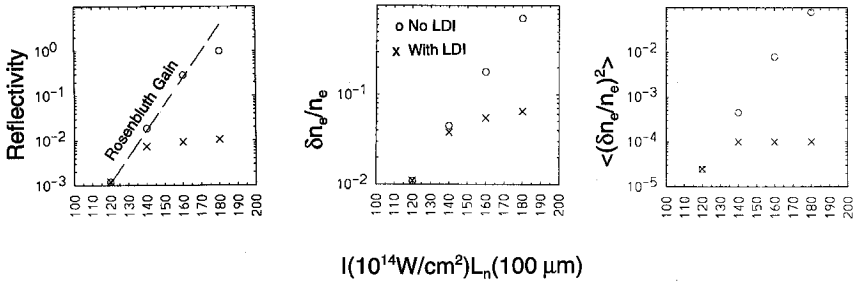

Figure 18

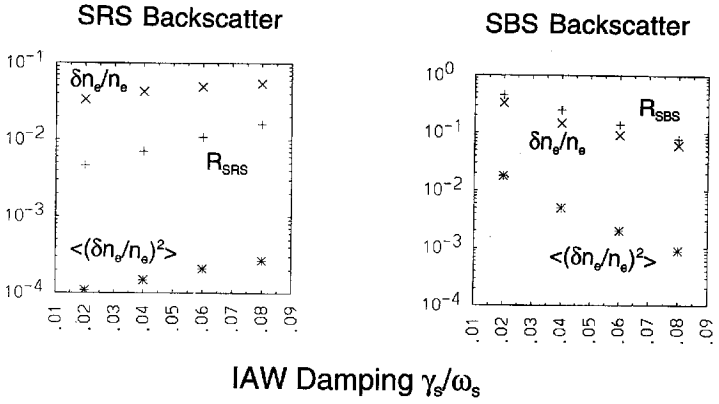

Figure 19

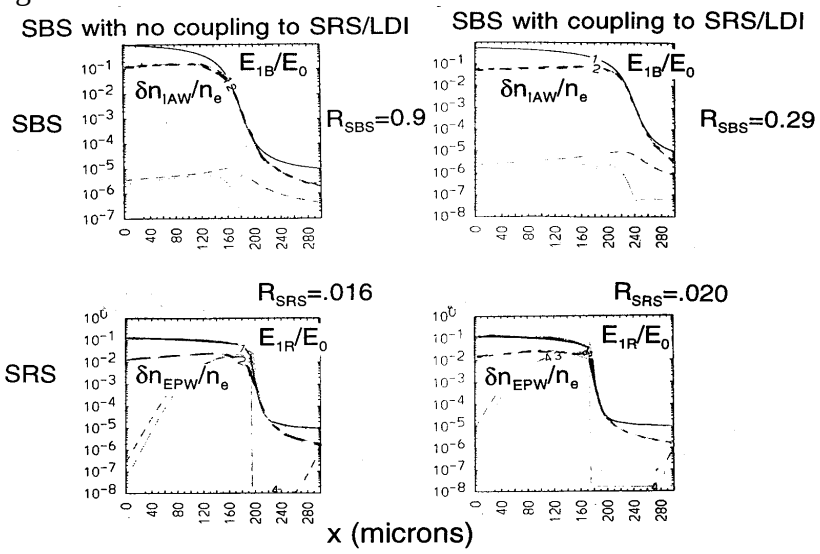

Figure 20

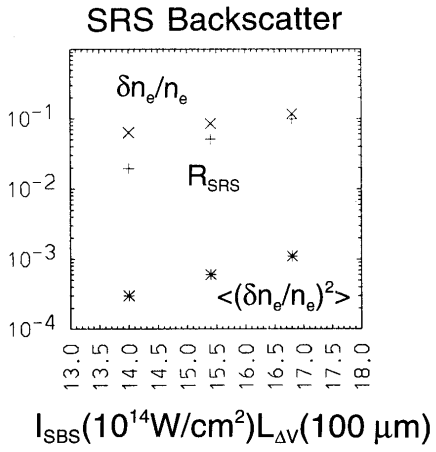

Fig. 21

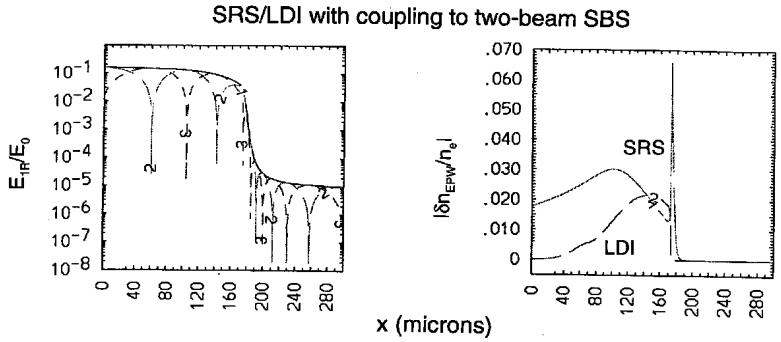

Figure 22

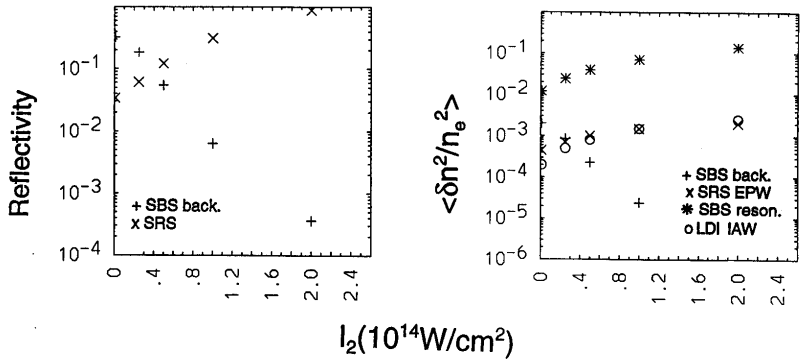

Figure 23

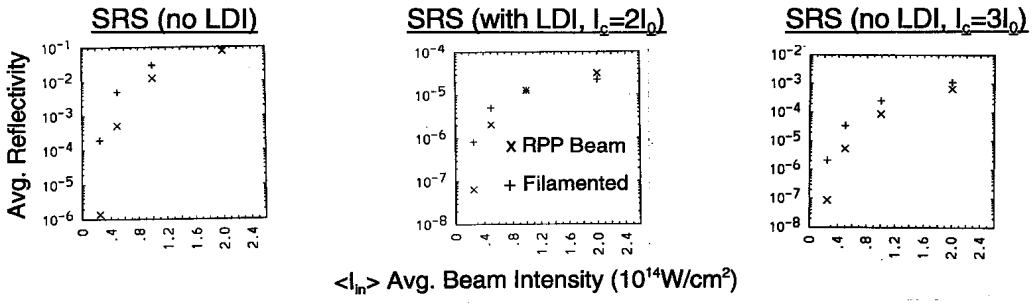

Figure 24

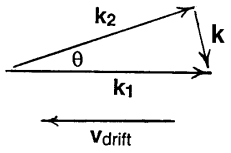

$\theta=22.5°$ $k \sim k_1 \sin\theta \sim 0.4\, k_1$

$\rightarrow$ $v_{drift} \sim c_s/0.4 \sim 2.5\, c_s$

Figure 25

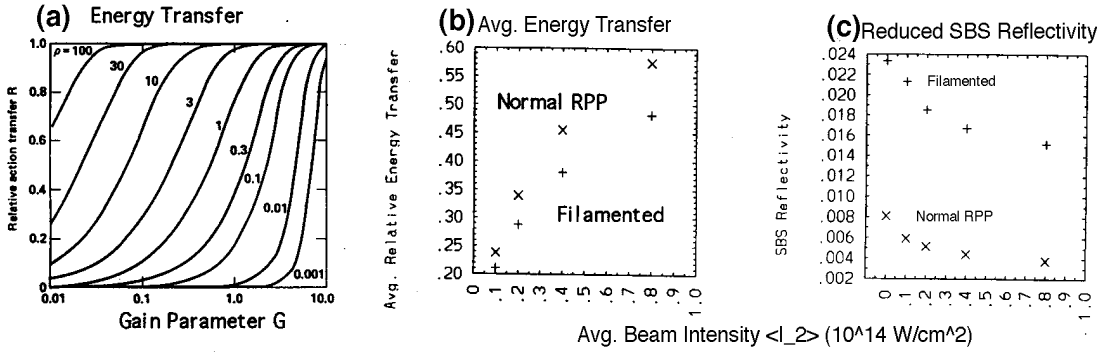
(a) Energy Transfer
Relative action transfer R
Gain Parameter G
ρ = 100
30
10
3
1
0.3
0.1
0.01
0.001
(b) Avg. Energy Transfer
Avg. Relative Energy Transfer
Normal RPP
Filamented
(c) Reduced SBS Reflectivity
SBS Reflectivity
Filamented
Normal RPP
Avg. Beam Intensity <I_2> (10^14 W/cm^2)